# Growth shapes and turbulent spots in unstable systems

Claudine V. Conrado and Tomas Bohr
*The Niels Bohr Institute, Blegdamsvej 17, 2100 Copenhagen Ø, Denmark*
(Received 30 September 1994)

We study the growth shapes of localized turbulent patches (turbulent spots) in a class of partial differential equations (PDE's) in two spatial dimensions, of first order in time and in one scalar field $u$. The PDE's are chosen such that the "laminar" state $u = 0$ is unstable, at least convectively (i.e., in a moving frame). We show which symmetry breaking terms are required to generate the characteristic nonconvex growth shapes found in turbulent spots in boundary layers, and how the shapes transform when we vary the coefficients of these terms. Finally, we show how it is possible, in certain cases, to find exact solutions for the nonlinear growth shapes and how to measure Lyapunov exponents of growing turbulent spots.

PACS number(s): 47.27.−i, 47.52.+j

## INTRODUCTION

It is a remarkable fact that the transition to turbulence in a shear flow near a wall can take place through the formation of *turbulent spots* or *Emmons spots* [1–3]. Small turbulent patches of a characteristic boomerang-like shape (in plan view) appear in the otherwise laminar flow (Fig. 1). As time passes the spot grows while it is advected by the mean flow such that, to a good approximation, the overall shape is invariant aside from translation and scaling [4, 5]. Thus, at least for a certain range in time, the spot has a well-defined *growth shape.*

The aim of the present work is to understand the origin and types of such nonconvex growth shapes. We will take a very simple but general approach: try to write down the simplest possible field theories possessing instabilities which will make a local disturbance grow convectively, and study the possible asymptotic shapes as well as the conditions under which they appear. Our starting point will be a class of unstable partial differential equations describing a large class of phenomena such as surface waves and chemical reactions. This class of equations does not include the Navier-Stokes equations, but even so we expect that our approach might be of interest also for the case of turbulent spots in shear flows. Experimental investigations of turbulent spots in boundary layers [4–6] make it clear that we are dealing with an extremely complex process, which is not understood in detail. Therefore a phenomenological approach similar to that of Landau might be reasonable: we think of the interior of the spot as having a nonzero "order parameter" (which we call $u$) which vanishes in the laminar fluid outside. This is, of course, a gross oversimplification, since the state in the spot cannot be described by a single scalar function and since the laminar state outside it is not steady. Nevertheless, we shall see that even the simple equations which we will study do give rise to interesting growth shapes and that, by varying the parameters in the equations, they change completely. Our paper can be seen as an extension to two dimensions of our previous work [7], in which similar problems were addressed in one dimension. In one dimension one can, of course, not find nontrivial growth shapes, but the nonlinear terms can create instabilities, just as in two dimensions.

The first part of the paper deals with shapes formed by *linear* unstable partial differential equations in two spatial dimensions. In principle it is well known how to find growth shapes in such systems [8–11]. For one-dimensional systems a large body of work has been done, but much less is known in higher dimensions. In works by Criminale and Kovasznay [12] and a series of works by Gaster [13], the shapes of localized disturbances in a laminar boundary layer were studied via the Orr-Sommerfeld equation. Our work can be seen as a generalization of their approach since, even though the Orr-Sommerfeld equation is not within the category of equations which we treat here, we can get very similar results. Moreover, since we are free to vary the parameters defining our equations, we can also obtain shapes which are completely different with interesting transitions between them.

In the second part of the paper we shall study the

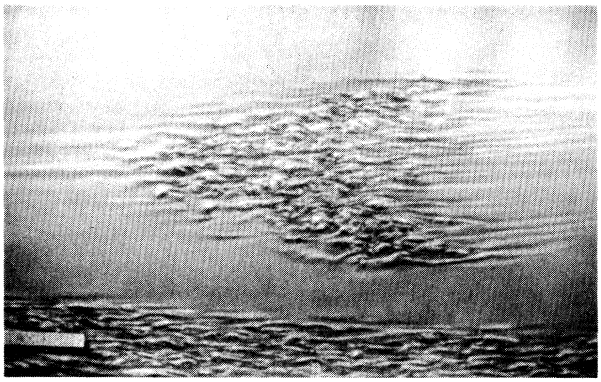

FIG. 1. Turbulent spot in water seen through a wall on which a boundary layer has formed. The flow is from left to right and the visualization by suspended aluminum flakes (from [5]).

 

effect of adding nonlinear terms to (1) (see below) and show how such terms can change the exponential growth inside the spot into turbulent fluctuations, without, in many cases, changing the growth shape. In other cases the nonlinear terms can create instabilities that destroy the self-similar growth shapes.

## I. GROWTH RATES AND GROWTH SHAPES IN LINEAR SYSTEMS

Our model equation is the following linear partial differential equation:

$$\frac{\partial u}{\partial t} = L_0\{u\} + L_1\{u\}, \tag{1}$$

where

$$L_0\{u\} = \chi u + a_0\nabla^2 u + b_0\nabla^4 u \tag{2}$$

and

$$L_1\{u\} = a_1\frac{\partial^2 u}{\partial {x_1}^2} + a_2\frac{\partial^2 u}{\partial {x_2}^2} + b_1\frac{\partial^4 u}{\partial {x_1}^4} + b_2\frac{\partial^4 u}{\partial {x_2}^4} + b_3\frac{\partial^4 u}{\partial {x_1}^2\partial {x_2}^2} + c_1\frac{\partial^3 u}{\partial {x_1}^3} + c_2\frac{\partial^3 u}{\partial x_1\partial {x_2}^2}, \tag{3}$$

with the $a_i$'s, $b_i$'s, $c_i$'s, and $\chi$ as constants. The operator $L_0$ has the full radial symmetry. In particular, it does not distinguish $x_1$ from $x_2$ nor $x_i$ from $-x_i$. Now, thinking of a planar turbulent spot, the mean flow selects a special direction, say $x_1$, and as a consequence it breaks the $x_1 \to x_2$ and $x_1 \to -x_1$ symmetries, whereas the $x_2 \to -x_2$ symmetry is retained. The operator $L_1$ has therefore, up to fourth order, *all* the symmetry breaking terms compatible with the symmetry of such systems.

Thus, in a shorthand notation, we have a linear partial differential equation describing the behavior in time and in space of a scalar field $u(\vec{x},t)$,

$$\frac{\partial u}{\partial t} = \phi\left(\frac{\partial}{\partial x_1}, \frac{\partial}{\partial x_2}\right)u, \tag{4}$$

where $\phi$ is an operator which is an arbitrary function of the spatial derivatives $\frac{\partial}{\partial x_1}$ and $\frac{\partial}{\partial x_2}$. Our model equation (1) is a special case of (4), in which the operator $\phi$ is a fourth-order polynomial in two variables. More generally, we can write $\phi$ as an expansion in powers of the operators $\frac{\partial}{\partial x_1} = D_1$ and $\frac{\partial}{\partial x_2} = D_2$,

$$\phi(D_1, D_2) = f_0 + f_1D_1 + f_2D_2 + f_3D_1^2 + f_4D_1D_2 + f_5D_2^2 + \cdots, \tag{5}$$

where the $f_i$'s are constants. If we further confine our attention to problems in which the $x_2 \to -x_2$ symmetry is present, we recover (1).

Starting from an initially localized disturbance, we now look for solutions to (4) which have the scaling form

$$u(\vec{x},t) \sim e^{\lambda(\frac{\vec{x}}{t})t} \tag{6}$$

in the limit of large $t$. The convective exponent $\lambda(\frac{\vec{x}}{t})$ will in general be complex and its real part $\lambda^r$ gives the asymptotic exponential growth or decay rate of the field $u$ for an observer moving with velocity $\vec{v} = \vec{x}/t$. An initially localized disturbance will diverge if $\mathrm{Re}[\lambda(\vec{v})]$ is positive for some $\vec{v}$. In this case, $\mathrm{Re}[\lambda(\vec{v})] = 0$ defines a curve in the $(v_1, v_2)$ plane, which gives the stationary growth shape of the disturbance. Such a shape is invariant in time as can be seen from (6): for all points on the curve [in $(x_1, x_2)$ space] the distance to the center (0,0) simply scales in time.

Substituting solution (6) in (4) and rewriting spatial derivatives as derivatives with respect to $\vec{v} = \vec{x}/t$, we find asymptotically [i.e., neglecting terms $o(1/t)$] that $\lambda(\vec{v})$ satisfies

$$\lambda(\vec{v}) = \vec{v}\cdot\vec{\nabla}_{\vec{v}}\lambda + \phi\left(\frac{\partial\lambda}{\partial v_1}, \frac{\partial\lambda}{\partial v_2}\right), \tag{7}$$

where $\phi$ is the function appearing in (4) which determines the model. This equation is the Clairaut equation [14] which can be solved by differentiating both sides of (7) with respect to $\vec{v}$. The general solution will be given by a *four*-parameter family of "planes,"

$$\lambda_{\vec{p}}(\vec{v}) = \vec{v}\cdot\vec{p} + \phi(p_1, p_2), \tag{8}$$

with the components $p_i$ of the vector $\vec{p}$ as arbitrary complex numbers. There are also solutions with no arbitrary constants — the singular solutions — which will be of interest since they can fulfill the important physical requirement that $\mathrm{Re}[\lambda(\vec{v})]$ should go to zero for sufficiently large $|\vec{v}|$. These solutions are obtained by eliminating $\vec{\nabla}_{\vec{v}}\lambda \equiv \vec{p}$ between (7) and

$$\vec{v} = -\vec{\nabla}_{\vec{p}}\phi, \tag{9}$$

which results from the differentiation procedure mentioned above. The elimination of $\vec{p}$ corresponds to first inverting (9) to obtain $\vec{p}(\vec{v})$ (this procedure will be referred to from now on as *inversion*) and second inserting this result back into (7) in order to find the dependence of $\lambda$ on $\vec{v}$.

The problem of finding asymptotic solutions to (4), starting from initially localized disturbances, can be formulated very directly in terms of Fourier integrals. For the Fourier component

$$u_{\vec{q}}(t) = \int d\vec{x}e^{-i\vec{q}\cdot\vec{x}}u(\vec{x},t), \tag{10}$$

Eq. (4) becomes

$$\frac{\partial u_{\vec{q}}}{\partial t} = \phi(iq_1, iq_2)u_{\vec{q}}. \tag{11}$$

Setting $\phi(iq_1, iq_2) = \nu_{\vec{q}}$, the solution to (11), when expressed again in terms of spatial coordinates, becomes

$$u(\vec{x},t) = \int d\vec{q}e^{(i\vec{q}\cdot\vec{x}+\nu_{\vec{q}}t)}u_{\vec{q}}(t=0), \tag{12}$$

with the limits of integration from $-\infty$ to $+\infty$ in both variables, $q_1$ and $q_2$.

We now set $\vec{x}$ equal to $(\vec{x_0} + \vec{v}t)$ in order to obtain the solution in a moving frame of reference. For sufficiently large $t$, the integral can then be evaluated by the saddle point method and we obtain an asymptotic expansion with respect to $t$. For an initially localized disturbance,

$u_{\vec{q}}(t=0)$ will be a smooth function of $\vec{q}$ and the main contribution to the integral will come from a saddle point of

$$f(\vec{q}) \equiv \nu_{\vec{q}} + i\vec{q}\cdot\vec{v}. \tag{13}$$

The problem now is to find all the saddle points of $f$ as functions of $\vec{v}$ and choose the *right* one (or right ones), that is, the one to which the path of integration, initially passing through the real axis, *can* be deformed without crossing singularities and which gives the largest contribution to the integral. The next step would be to expand the function $f$ around the saddle point thus obtaining an asymptotic expansion with respect to $t$. However, in the present work we will only be interested in the exponential approximation for the integral, which has the form $u \sim e^{f(\vec{q}_0(\vec{v}))t}$, equivalent to (6). Here $\vec{q}_0$ represents the *right* saddle point and $f(q_0(\vec{v}))$ is simply what we earlier called $\lambda(\vec{v})$.

We observe that the inversion defined in terms of (9) corresponds to the problem of finding the saddle points of $f(\vec{q})$ in (13). As a matter of fact, (9) with $\vec{p} = i\vec{q}$ is exactly the equation which determines the saddle points with $\phi(iq_1, iq_2) = \nu_{\vec{q}}$. This equation will in general have more than one solution for each value of $\vec{v}$, so that the choice of the right saddle point must involve an analysis of the behavior of $f(\vec{q})$ around each of them. When the problem involves functions of *one* complex variable this analysis is relatively easy. In the present case, however, working with *two* complex variables, the choice of the right saddle point for an isolated value of $\vec{v}$ is not always clear. Instead we follow the contribution from all saddles for all $\vec{v}$. We can then look at the real part $\lambda^r(\vec{v})$ from each and ask for the *well-behaved* one(s): the one(s) that go(es) to $-\infty$ when $v = |\vec{v}|$ becomes large. As we will see later, the choice of the well-behaved $\lambda^r(\vec{v})$ might imply that one has to change from one solution $\vec{p}(\vec{v})$ to another when the corresponding solutions $\lambda^r(\vec{v})$ cross. Since $\vec{p} = \vec{\nabla}_{\vec{v}}\lambda$, the change will correspond to a discontinuity in the slope of $\lambda(\vec{v})$, although the function itself is continuous.

### A. Examples with radial symmetry

In order to show how the formalism works and introduce important examples for later generalization, we will now treat two examples in which complete radial symmetry is present. We shall therefore consider only $L_0$ in our model equation (1) and, consequently, all growth shapes will be circular.

As our first and simplest example we discuss the symmetric diffusion equation which can be made unstable by the addition of a term linear in $u$. Taking $a_0 = 1$ and $b_0 = 0$ in (2), the equation for $u$ becomes

$$\frac{\partial u}{\partial t} = \chi u + \nabla^2 u \tag{14}$$

and thus the function $\phi$, defined in (4), is the simple second-degree polynomial $\phi(p_1, p_2) = \chi + p^2$, where $p = |\vec{p}|$. In this case, inversion is trivial:

$$v_i = -\frac{\partial \phi}{\partial p_i} \tag{15}$$

leads directly to

$$p_i = -\frac{1}{2}v_i, \tag{16}$$

whereby we find

$$\lambda(\vec{v}) = \phi + v_i p_i = \chi - \frac{v^2}{4}, \tag{17}$$

where $v$ denotes $|\vec{v}|$.

In this first example $\lambda(\vec{v})$ is real, but this will not be the case if higher order derivatives are present in the equation for $u$. In any case, the information concerning the stability of a disturbance is contained in the real part of $\lambda(\vec{v})$. The interesting situation is the unstable one, in which $\chi$ is positive. In this case, an initially localized disturbance will grow or decay exponentially with growth rates varying from the maximum value $\chi$ to $-\infty$, depending on the velocity of the moving frame of reference from which one observes. In the unstable cases in general, $\mathrm{Re}[\lambda(\vec{v})]$ will have this kind of behavior: positive in some finite region of the $(v_1, v_2)$ plane, but going to $-\infty$ for large enough $v = |\vec{v}|$. The values of $(v_1, v_2)$ for which $\mathrm{Re}[\lambda(\vec{v})] = 0$ — the neutral stability curve—will then define the growth shape of the disturbance. In this simple example, the shape is given as the circle $v = 2\sqrt{\chi}$. Further, since $\vec{v} = \vec{0}$ is in the unstable region (14) is *absolutely unstable*.

Our second radially symmetric example is a model with higher derivatives, which is obtained from (2) with $\chi = 0$, $a_0 = -1$, and $b_0 = 1$:

$$\frac{\partial u}{\partial t} = -\nabla^2 u - \nabla^4 u. \tag{18}$$

This is the type of linear equation appearing in systems with "negative surface tension," for example, the Kuramoto-Sivashinsky equation [15, 16] or the Swift-Hohenberg equation [17]. Here the function $\phi(\vec{p})$ has the form

$$\phi(\vec{p}) = -p^2 - p^4 \tag{19}$$

and, due to the presence of the term $p^4$, the inversion becomes nontrivial. Using (9), we find that $p_i = \frac{v_i}{v}p(v)$, where $p(v)$ satisfies

$$4p^3 + 2p = v. \tag{20}$$

This equation is a third-degree polynomial in $p$ which has one real and a pair of complex conjugate roots. It is easy to see that the path of integration can be deformed in order to pass over the complex roots in the direction of steepest descent, whereas it cannot for the real root. Thus only the complex conjugate pair contributes and the solution can be written explicitly as

$$p(v) = -\frac{1}{2}(s_+ - s_-) \pm i\frac{\sqrt{3}}{2}(s_+ + s_-), \tag{21}$$

where

$$s_\pm = \frac{1}{2}\left(\sqrt{v^2 + \frac{8}{27}} \pm v\right)^{\frac{1}{3}} \tag{22}$$

and we can calculate $\lambda(v)$ as

$$\lambda(v) = \phi + v_i p_i = 3p^4 + p^2. \tag{23}$$

The real part of $\lambda(v)$ is positive around the origin and attains its maximal value 0.25 for $\vec{v} = \vec{0}$. It decreases as $v$ becomes large, defining the circle $v \approx 1.6$ as the growth shape.

It is instructive to understand the choice of the right solution $p(v)$ from the procedure described in the end of the previous section. The complex conjugate pair solution will give the *well-behaved* $\lambda^r(v)$ discussed above. The real solution, on the other hand, will give a $\lambda^r(v)$ which goes to $+\infty$ as $v$ increases from zero. This behavior is obviously unphysical and therefore the complex conjugate pair is the right solution.

The imaginary part of $\lambda(v)$, $\lambda^i(v)$, is different from zero and when that is the case there will be oscillations superimposed with the profile determined by the real part, whose wave vector is given by $\vec{\nabla}_{\vec{v}}\lambda^i(\vec{v})$. In the present example, $\lambda^i(\vec{v})$ has a conical shape, which gives a radially symmetric wave vector whose modulus is approximately constant ($\approx 1/\sqrt{2}$) over the range of values of positive $\lambda^r(v)$.

### B. Perturbation expansion for growth shapes

If the symmetry breaking terms $L_1$ given in (3) are small compared to $L_0$, we might attempt to find the growth shapes perturbatively, starting from the circular ones given by $L_0$.

Assume that we have an equation with a $\phi$ of the form

$$\phi = \phi_0(\vec{p}) + \epsilon\phi_1(\vec{p}), \tag{24}$$

where $\epsilon\phi_1$ is small compared to $\phi_0$. The parameter $\epsilon$ is a *formal* parameter, which means we will do the analysis in powers of $\epsilon$, but in the end it will be set to $\epsilon = 1$.

According to (9), the velocities are given by

$$v_i = -\frac{\partial\phi}{\partial p_i} = -\frac{\partial\phi_0}{\partial p_i} - \epsilon\frac{\partial\phi_1}{\partial p_i} \tag{25}$$

and for small $\epsilon$ the solution $p_i(\vec{v})$ of (25) can be expanded as

$$p_i(\vec{v}) = p_i^0(\vec{v}) + \epsilon p_i^1(\vec{v}) + \epsilon^2 p_i^2(\vec{v}) + \cdots = p_i^0(\vec{v}) + \delta p_i(\vec{v}). \tag{26}$$

But the velocities can also be found from the unperturbed variables as

$$v_i = -\frac{\partial\phi_0}{\partial p_i^0}. \tag{27}$$

Thus, equating (25) and (27) we find

$$\frac{\partial^2\phi_0}{\partial p_i^0\partial p_j^0}\delta p_j + \frac{1}{2}\frac{\partial^3\phi_0}{\partial p_i^0\partial p_j^0\partial p_k^0}\delta p_j\delta p_k + \cdots + \epsilon\frac{\partial\phi_1}{\partial p_i^0}$$

$$+\epsilon\frac{\partial^2\phi_1}{\partial p_i^0\partial p_j^0}\delta p_j + \frac{1}{2}\epsilon\frac{\partial^3\phi_1}{\partial p_i^0\partial p_j^0\partial p_k^0}\delta p_j\delta p_k + \cdots = 0, \tag{28}$$

where $\delta p_i = \epsilon p_i^1 + \epsilon^2 p_i^2 + \cdots$ and summation over $j$ and $k$ is implied. Now we can calculate $\lambda(\vec{v}) = \phi + v_i p_i$. By expanding and using again $v_i = -\frac{\partial\phi_0}{\partial p_i^0}$ we find

$$\lambda = \phi_0(p^0) + v_i p_i^0 + \epsilon\phi_1 + \frac{1}{2}\frac{\partial^2\phi_0}{\partial p_i^0\partial p_j^0}\delta p_i\delta p_j + \cdots$$

$$+\epsilon\frac{\partial\phi^1}{\partial p_i^0}\delta p_i + \epsilon\frac{1}{2}\frac{\partial^2\phi_1}{\partial p_i^0\partial p_j^0}\delta p_i\delta p_j + \cdots, \tag{29}$$

which, to lowest order in $\epsilon$, becomes $\lambda = \lambda^0 + \epsilon\phi_1[\vec{p}^{\,0}(\vec{v})]$.

For the higher orders in $\epsilon$, the result will depend explicitly on the correction $\delta p_i$. In second order we need $\delta p_i$ to first order, i.e., $\delta p_i \simeq \epsilon p_i^1$. From (29) we obtain

$$\lambda = \lambda^0 + \epsilon\phi_1 + \epsilon^2\left(\frac{\partial\phi^1}{\partial p_i^0}p_i^1 + \frac{1}{2}\frac{\partial^2\phi_0}{\partial p_i^0\partial p_j^0}p_i^1 p_j^1\right), \tag{30}$$

where $p_i^1$ is found from (28):

$$\frac{\partial^2\phi_0}{\partial p_i^0\partial p_j^0}p_j^1 = -\frac{\partial\phi_1}{\partial p_i^0}. \tag{31}$$

When this is inserted back into (30) we find

$$\lambda = \lambda^0 + \epsilon\phi_1 + \frac{1}{2}\epsilon^2\frac{\partial\phi^1}{\partial p_i^0}p_i^1. \tag{32}$$

The equation for $p_i^1$ in (31) is a linear equation. If we denote the derivatives of $\phi_0$ and $\phi_1$ as

$$M_{ij} = \frac{\partial^2\phi_0}{\partial p_i^0\partial p_j^0}, \qquad L_i = \frac{\partial\phi_1}{\partial p_i^0}, \tag{33}$$

Eq. (31) becomes

$$M_{ij}p_j^1 = -L_i \tag{34}$$

with the solution $p_i^1 = -(M^{-1})_{ij}L_j$. Finally setting $\epsilon = 1$ we obtain

$$\lambda = \lambda^0 + \phi_1 - \frac{1}{2}(M^{-1})_{ij}L_iL_j, \tag{35}$$

which gives $\lambda(\vec{v})$ to second order in the perturbation amplitude.

We now apply the results obtained above to perturbations of the two radially symmetric models, (14) and (18), discussed in the previous section. We will consider in both examples the same perturbative term

$$\phi_1 = a_1p_1^2 + c_1p_1^3 + c_2p_1p_2^2 \tag{36}$$

as obtained from (3) with $a_2 = b_i = 0$.

As the first application, let us consider the model given in (14) for which $\phi_0 = \chi + p^2$ (case 1). We need to calculate the quantities $M_{ij} = 2\delta_{ij}$, $L_1 = 2a_1p_1 + 3c_1p_1^2 + c_2p_2^2$ and $L_2 = 2c_2p_1p_2$. To order $\epsilon$,

$$p_1^1 = -\frac{1}{2}\frac{\partial\phi_1}{\partial p_1} = -a_1p_1 - \frac{3}{2}c_1{p_1}^2 - \frac{1}{2}c_2p_2^2,$$

$$p_2^1 = -\frac{1}{2}\frac{\partial\phi_1}{\partial p_2} = -c_2p_1p_2, \tag{37}$$

where we have dropped the superscript 0 on the $p$'s. From (35), after expressing the $p_i$'s in terms of the $v_i$'s by $p_i = p_i^0 = -\frac{1}{2}v_i$, finally we obtain

$$\lambda(v_1,v_2)=\lambda^0(v)+\frac{a_1(1-a_1)}{4}v_1^2-\frac{c_1}{8}(1-3a_1)v_1^3 -\frac{c_2}{8}(1-a_1)v_1v_2^2-\frac{9c_1^2}{64}v_1^4-\frac{c_2^2}{64}v_2^4 -\frac{c_2}{16}\left(\frac{3}{2}c_1+c_2\right)v_1^2v_2^2, \tag{38}$$

where $\lambda^0(v)$ is given in (17).

The other example is the model given in (18) for which $\phi_0=-p^2-p^4$ (case 2). Now the matrix of second derivatives of $\phi^0$ is

$$M=\begin{bmatrix}2(1+2p^2)+8(p_1)^2 & 8p_1p_2\\ 8p_1p_2 & 2(1+2p^2)+8(p_2)^2\end{bmatrix} \tag{39}$$

and, as before, $L_1=2a_1p_1+3c_1p_1^2+c_2p_2^2$ and $L_2=2c_2p_1p_2$. The matrix $M^{-1}$ is then given by

$$M^{-1}=\frac{1}{D}\begin{bmatrix}2(1+2p^2)+8(p_2)^2 & -8p_1p_2\\ -8p_1p_2 & 2(1+2p^2)+8(p_1)^2\end{bmatrix}, \tag{40}$$

where $D=4(1+2p^2)(1+6p^2)$ is the determinant of $M$. It is easy to show that $D$ never vanishes and therefore the inverse $M^{-1}$ always exist. When these expressions are inserted into (35), we obtain $\lambda$ expressed in terms of the $p_i$'s with $\lambda^0=p^2+3p^4$. Next, we have to express everything in terms of the $v_i$'s using the relations found earlier for the unperturbed system. As noted in the previous section, $p_i=\frac{v_i}{v}p(v)$ with the solution $p(v)$ given by (21) and (22). Finally, the growth shape is determined from the equation $\lambda^r(\vec{v})=0$.

In Figs. 2 and 3 we show level curves for $\lambda^r(\vec{v})$ for the cases 1 and 2, respectively. In both cases the circular shapes distort due to the symmetry breaking terms in $\phi_1$. In the first case, however, these distortions never lead to nonconvex shapes, whereas for the second case there will always be nonconvex contours, even for small values of $a_1$ and $c_i$. This is due to the fact that $\lambda^r(\vec{v})$ is singular around $\vec{v}=\vec{0}$ as will be shown.

When (22) is inserted into (21), we find the following expansions (through order $v^2$):

$$p_i(\vec{v})\approx\frac{v_i}{v}\left[-\frac{1}{4}v+\frac{i}{\sqrt{2}}\left(1+\frac{3}{16}v^2\right)\right], \tag{41}$$

$$p^2(\vec{v})\approx-\frac{1}{2}-\frac{1}{8}v^2-\frac{i}{2\sqrt{2}}v. \tag{42}$$

Note that in this case $p^2$ does not vanish as $v\to 0$. Further,

$$p^4(\vec{v})\approx\frac{1}{4}+\frac{i}{2\sqrt{2}}v \tag{43}$$

and

$$\lambda_0^r(\vec{v})\approx\frac{1}{4}-\frac{1}{8}v^2. \tag{44}$$

Let us first suppose that $c_1=c_2=0$. Then the perturbation expansion to first order becomes

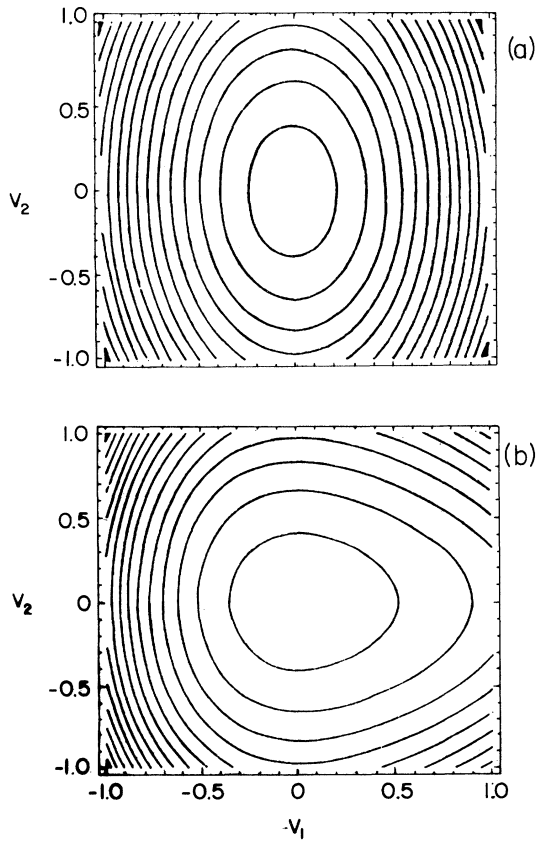


FIG. 2. Level curves for $\lambda^r(\vec{v})$ as obtained from perturbation theory for the case of positive Laplacian (case 1). (a) $a_1=2$ and $c_1=c_2=0$ and (b) $a_1=c_1=c_2=1$.

$$\lambda^r(\vec{v})\approx\frac{1}{4}-\frac{1}{8}v^2-\frac{a_1}{8}v_1^2-\frac{a_1}{2}\left(\frac{v_1}{v}\right)^2. \tag{45}$$

The last term can create singular behavior since it does not vanish as $v\to 0$. In polar coordinates — $v_1=v\cos\theta$ and $v_2=v\sin\theta$ — we can solve for the level curves of (45) ($\lambda=\Lambda_0$), and for simplicity neglecting the $v_1^2$ term we obtain

$$r(\theta)\approx\sqrt{8\left(C-\frac{a_1}{2}\cos^2\theta\right)}, \tag{46}$$

where $C=\frac{1}{4}-\Lambda_0$. When $a_1>2C$ the contour is singular, passing twice through zero at angles $\pm\alpha$ and $\pi\pm\alpha$, where $\alpha=\cos^{-1}\sqrt{2C/a_1}$. Typically, level curves on a surface would only have such singular shapes for isolated parameter values. Small changes in the parameter would either result in a simple (nonconvex) curve or two disjoint closed curves. The reason for the strange behavior is that the surface in (45) is not defined at $r=0$. The limiting value for $r\to 0$ depends on $\theta$. For $a_1<2C$, the contours are indeed simple closed curves with nonconvex parts (*violin* shape).

When the $c$ terms are added, no new singularities are encountered. The simplest case is $c_1=c_2=c$. Again

neglecting the $v_1^2$ term, we find

$$r(\theta) = \frac{3}{2}c\cos\theta \pm \sqrt{8C + (\tfrac{9}{4}c^2 - 4a_1)\cos^2\theta}, \quad (47)$$

where the sign is chosen such that $r \geq 0$. Now, the $\frac{3}{2}c\cos\theta$ term moves the front end forwards and the back end backwards, so a nonconvex, boomerang-shaped spot is formed for $8C > 4a_1 - \frac{9}{4}c^2$.

This is seen more clearly when $c_1 \neq c_2$. In this case (45) becomes

$$\lambda \approx \frac{1}{4} - \frac{v^2}{8}(1 + a_1\cos^2\theta) - \frac{a_1}{2}\cos^2\theta + B(\theta)v, \quad (48)$$

where

$$B(\theta) = \frac{1}{16}[(c_1 - c_2)\cos 3\theta + (3c_1 + c_2)\cos\theta]. \quad (49)$$

The level curves of $\lambda$ for this case are shown in Fig. 3(c).

As we saw, it is possible to obtain shapes very much like the turbulent spot, even within lowest order perturbation theory for the case with negative Laplacian (case 2). We expect the perturbation theory to be valid only sufficiently far from the origin [i.e., for $y^2 >$ const $\times a_1$ in (45)] since the perturbative corrections dominate at the origin and create an ill-defined $\lambda(\vec{v})$ surface. As we shall see in the next section, the reason for the singular behavior is the *degeneracy* of the case $a_1 = c_1 = c_2 = 0$. As soon as the system is perturbed, a new solution appears, which must be properly taken into account.

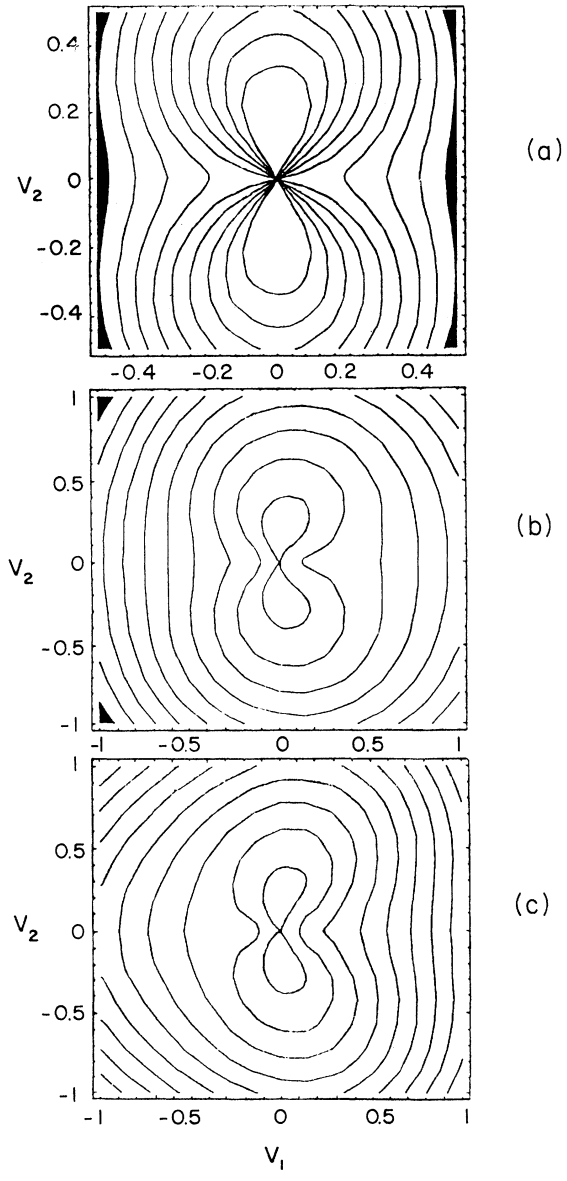


FIG. 3. Same as Fig. 2 for the case of negative Laplacian (case 2). (a) $a_1 = 0.5$ and $c_1 = c_2 = 0$, (b) $a_1 = c_1 = c_2 = 0.5$, and (c) $a_1 = 0.5$, $c_1 = -0.5$, and $c_2 = 0.5$.

### C. Full solution of the basic model

In the present section we shall discuss in detail the calculation of $\lambda(\vec{v})$ for the model equation defined by (1), which corresponds to the expansion of the operator $\phi$ in (5) up to fourth order in the operators $D_1$ and $D_2$. For simplicity we shall confine our attention to the case defined by (4) where the operator $\phi$ is given by

$$\phi(D_1, D_2) = \chi - (1 - a)D_1^2 - D_2^2 - (D_1^2 + D_2^2)^2 + cD_1(D_1^2 + D_2^2). \quad (50)$$

The role played by the constant $\chi$ is simply to shift the whole surface $\lambda(\vec{v})$ up or down, so by changing its value we can obtain different growth shapes for a given surface $\lambda^r(\vec{v})$. This procedure is equivalent to disregarding $\chi$ and redefining the growth shapes as any level curve of $\lambda^r(\vec{v})$. We observe that our model, defined through (50), will be unstable only if $\chi > -\frac{1}{4}$.

As discussed earlier, Eq. (4) can be solved by a decomposition into Fourier modes and a subsequent integration back to the space of coordinates. Transforming to a frame of reference moving with velocity $\vec{v}$, the Fourier integral can be written as

$$I(\vec{v}, t) = \int d\vec{q} e^{f(\vec{q})t} U(\vec{q}), \quad (51)$$

where $f(\vec{q})$ is defined in (13) and $U(\vec{q})$ is assumed to be a smooth function of $\vec{q}$. The eigenvalue $\nu(\vec{q})$ (or complex dispersion relation) is obtained from (50) with the substitution $D_k \to iq_k$ and $f(\vec{q})$ becomes

$$f(\vec{q}) = [\chi + (1 - a)q_1^2 + q_2^2 - q^4] + i(v_1 q_1 + v_2 q_2 - cq_1 q^2), \quad (52)$$

where $q = |\vec{q}|$. In order to evaluate the integral in (51), we must now find the saddle points of $f$, which is taken as a function of the complex variables $q_1$ and $q_2$. If we choose the right one, say $\vec{q_0}(\vec{v})$, then the integral can be estimated as $I(\vec{v}, t) \sim e^{f(\vec{q_0}(\vec{v}))t} = e^{\lambda(\vec{v})t}$. Before developing this calculation, however, we will look at the real saddle points of $f(\vec{q})$, which can give some interesting information about $\lambda^r(\vec{v})$.

### 1. The real saddle points of $f(\vec{q})$

We observe that if $f(\vec{q})$ has a real saddle point, it will be a critical point of its real and imaginary parts as functions of real $\vec{q}$. We then start by looking at the expression for $f$ in (52) as a function of real $q_i$. The real part of $f$ is a fourth-degree polynomial in the two real variables and it must have at least one global maximum since for large enough $|q_i|$ it falls to $-\infty$. More generally, the global maxima can be degenerate and saddle points (in this context meaning one of the possible critical points of a real function of two real variables) may also be present. The global maximum of the real part is important since it actually *is* the right saddle point contributing to the integral at the velocity whose components are

$$v_1 = c(3q_{1m}^2 + q_{2m}^2),$$
$$v_2 = 2cq_{1m}q_{2m}. \tag{53}$$

This is the group velocity of the wave packet [18] and it is found as the velocity which makes the imaginary part of $f(\vec{q})$ stationary (to first order) at $\vec{q}_m$. Moreover, since the saddle point is real in this case, the gradient with respect to $\vec{v}$ of $\lambda^r(\vec{v})$ (which equals $\vec{p}^{\,r} = -\vec{q}^{\,i}$) vanishes and, in fact, it can be shown (see the Appendix) that $\lambda^r(\vec{v})$ is a maximum at that velocity. A similar result is also true for other critical points of Re[$f$] which *may* contribute at the corresponding velocities given by (53), as shown in the Appendix. Therefore, from a simple inspection of the real part of $f(\vec{q})$ and a determination of its global maxima, we can find the points in the $(v_1, v_2)$ plane of largest growth rate for the disturbance as well as the value of this quantity. Furthermore, other critical points of Re[$f$] besides the global maxima may be the contributing saddle points at the corresponding velocities.

We now go back to $f(\vec{q})$ in (52) and look at the critical points — maxima and saddle points — of Re[$f$] for real $q_i$. We note that there is a local minimum at the origin, which nevertheless never contributes. When $a = 0$, Re[$f$] has its maximum value $\chi + \frac{1}{4}$ for values of $\vec{q}$ on a circle around the origin. For nonzero $c$, this degeneracy will be brought through (53) into the $(v_1, v_2)$ plane, where points on a circle with its center displaced from the origin in the $v_1$ direction — the value of this displacement depending on the values of $c$ — will all have the same maximum exponential growth rate. For points in the $(v_1, v_2)$ plane which lie inside and outside the circle, the growth rate will of course be smaller and an interesting annular growth shape can be obtained for values of $\chi$ slightly above $-\frac{1}{4}$. When this value is increased, which correspond to taking lower level curves of the surface, we expect that shape to change since its particular feature comes from the degeneracy of the *maximum* of $\lambda^r(\vec{v})$. The simplest possible transition is to a single closed curve, through the shrinking of the inner curve, as shown in Fig. 4(a). The situation, shown in Fig. 4(b), in which the inner closed curve touches the outer one at the point $S$, is not possible. $S$ would then be a saddle point and we know from the Appendix that the surface $\lambda^r(\vec{v})$ cannot have a saddle point in this case. For $c = 0$, the circle in the $(v_1, v_2)$ plane collapses to the origin $\vec{v} = \vec{0}$ and we are back to one of the radially symmetric cases of Sec. II with trivial growth shapes.

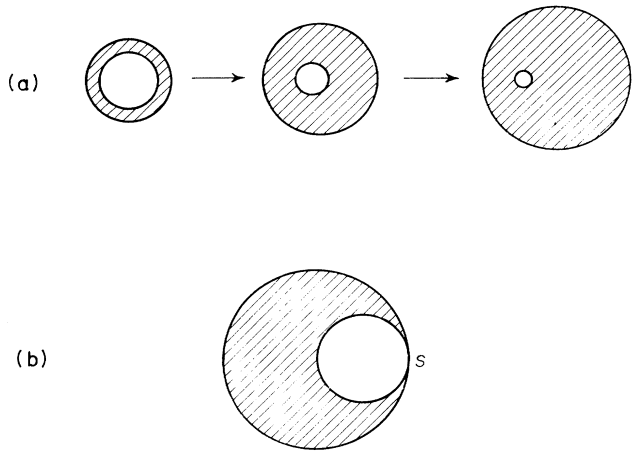


FIG. 4. (a) Transition sequence between shapes for the model described by (50) with $a = 0$ and nonzero $c$. (b) Growth shape corresponding to the level curve of $\lambda(\vec{v})$ through the saddle point. The exponentially growing parts are hatched and the saddle point is labeled S.

For nonzero $a$, say positive, the degeneracy is broken and Re[$f$] will have two global maxima in the $q_2$ axis ($q_{1m} = 0$) and two saddle points in the $q_1$ axis. For nonzero $c$, the group velocity lies on the $v_1$ axis as can be seen from (53). The two saddle points of Re[$f$] *may* also contribute at the corresponding velocity given by (53), since they are critical points of Re[$f$] as well. If this is the case, $\lambda^r(\vec{v})$ will also have a saddle point at that velocity, as shown in the Appendix. We now have the possibility of obtaining interesting growth shapes. For example, the shape shown in Fig. 4(b) is now possible, since we may have a saddle point on the surface $\lambda^r$. In Fig. 5, we show a possible transition between shapes for the present case which includes the shape shown in Fig. 4(b): lower level curves give the same transition sequence as shown in Fig. 4(a), but the higher ones show an interesting shape with a concave part, similar to the boomeranglike shapes of turbulent spots. On the other hand, if $c = 0$ the group velocity is zero, but also the velocity at which the saddle points of Re[$f$] might contribute as a saddle point of $f$ [see (53)]. Therefore the saddle point does not contribute and $\lambda^r$ has a maximum at $\vec{v} = \vec{0}$. The growth shapes are, however, nontrivial as we will see in the next subsection.

### 2. The complex saddle points of $f(\vec{q})$

We now proceed to the calculation of $\lambda(\vec{v})$ for all $\vec{v}$. The saddle points of $f(\vec{q})$ in (52) are the points $(q_1, q_2)$ in the complex plane which satisfy the equations

$$\frac{\partial f}{\partial q_1} = 2(1-a)q_1 - 4q_1^3 - 4q_1q_2^2 + iv_1 - 3icq_1^2 - icq_2^2 = 0,$$
$$\frac{\partial f}{\partial q_2} = 2q_2 - 4q_2^3 - 4q_1^2q_2 + iv_2 - 2icq_1q_2 = 0. \tag{54}$$

The maximum possible number of solutions for this system of algebraic equations is nine for given values of $a$,

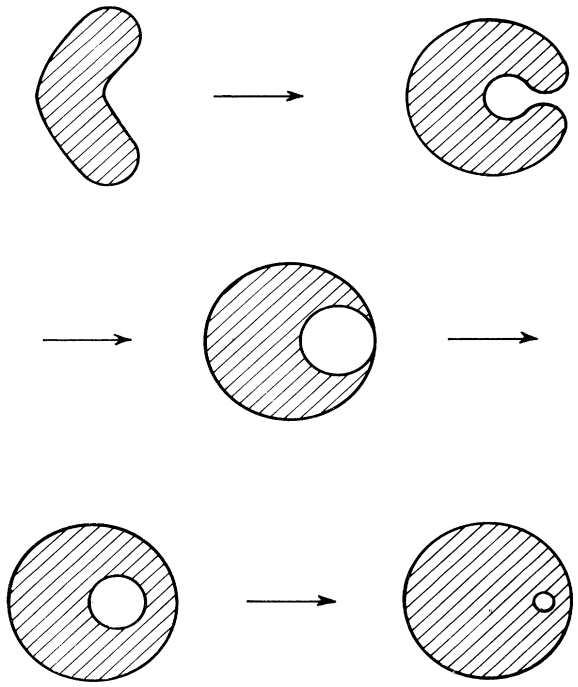

FIG. 5. Sequence of growth shapes corresponding to (50) with nonzero $a$ and $c$. The exponentially growing parts are hatched.

$c$, and $v_i$, since each equation is cubic in either of the variables. However, the symmetry of the equations reduces this number as we can see from the example with radial symmetry in (18). In this case, $a = c = 0$ and the system of two equations reduces to the cubic equation (20) for $p$ $(= iq)$ and $p_i(v) = \frac{v_i}{v} p(v)$. Thus, there are only three solutions, two of which are a complex conjugate pair. In the present case, we have to solve the system (54) explicitly. Solving the first equation for $q_2^2$ and inserting the result into the second equation gives an algebraic equation of fifth degree in $q_1$, whose solutions can be found numerically and the corresponding $q_2$'s can be determined. There are therefore five saddle points $(q_1, q_2)$ for each value of $\vec{v}$. This result is still true if $a = 0$ or $c = 0$ in (54). In this sense, the two asymmetries are similar and, as will be seen, give rise to the same type of structure in $\lambda(\vec{v})$.

In order to gain some understanding of the behavior of the solutions, we look at the system (54) with $v_2 = 0$. In this case, three of the solutions will be $(q_1^{(i)}, 0)$, where the $q_1^{(i)}$'s are roots of the cubic equation

$$2(1-a)q_1 - 4q_1^3 + iv_1 - 3icq_1^2 = 0 \tag{55}$$

and the two others are

$$q_1 = i\frac{2v_1 - c}{4a + c^2}, \qquad q_2 = \pm\sqrt{1 - {q_1}^2 - i\frac{c}{2}q_1}. \tag{56}$$

Thus we can say that there are two different kinds of saddle points, coming from either (55) or (56). As in the radial symmetric example mentioned above, the solutions of the cubic equation (55) will correspond to two solutions $\lambda^r(v_1, v_2 = 0)$: one which comes from the contribution of a complex conjugate pair of roots and goes to $-\infty$ as $|v_1|$ becomes large — a *well-behaved* solution — and another which diverges for large $|v_1|$. However, the two saddles in (56) also correspond to a well-behaved solution, which turns out to have the very simple form

$$\lambda^r(v_1, v_2 = 0) = \frac{1}{4}\left(1 - \frac{(2v_1 - c)^2}{4a + c^2}\right). \tag{57}$$

These solutions are shown in Fig. 6 for three distinct asymmetric cases which we shall consider below. As can be seen, the solutions cross each other which gives us the possibility of changing from the saddle point of one kind to the saddle point of another kind without creating discontinuities in $\lambda(\vec{v})$.

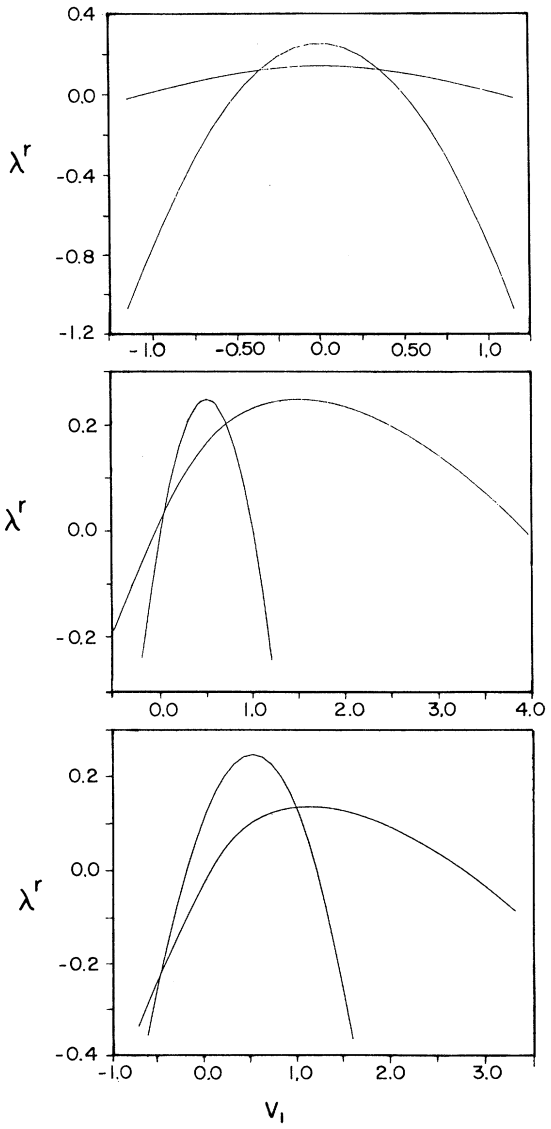


FIG. 6. $\lambda^r(v_1, v_2 = 0)$ for (a) $a = 0.25$ and $c = 0$, (b) $a = 0$ and $c = 1$, and (c) $a = 0.25$ and $c = 1$. The solutions correspond to well-behaved contributions from the saddle points in (55) and (56).

We now look at the saddle points for a generic value of $(v_1, v_2)$. They can be found numerically from the roots of a fifth-order algebraic equation, as mentioned above, and the corresponding convective exponents can be obtained. In Fig. 7, we show $\lambda^r(\vec{v})$ for $a = 0.25$ and $c = 0$. Due to the $v_i \to -v_i$ symmetry of the problem, only the region of the $(v_1, v_2)$ plane for which $v_1 > 0$ and $v_2 > 0$ is shown. Figure 7(a) shows the surface obtained from the parabolic solution in (57). In Fig. 7(b), the same is shown for the other well-behaved solution. They were obtained in this way by following the respective saddle points for increasing $v_2$. The physical solution, which is shown in Fig. 8(a), can be obtained as a single-valued function by taking the right branch of $\lambda^r(\vec{v})$ (the one which decreases for large $v$). The surface has a discontinuity in its first derivative, which corresponds to changing saddle points. At the branch points, marked by dots in Fig. 8(a), the saddle points of different kinds merge together and the solution becomes smooth. The other branch of $\lambda^r(\vec{v})$ has a saddlelike structure: for large $v$, it goes to $-\infty$ in the $v_1$ direction, whereas it diverges in the $v_2$ direction.

The results obtained above, concerning the general structure of $\lambda^r(\vec{v})$, do not depend on the specific numerical values of $a$ and $c$, provided that they are not both zero. This can be seen from the solution (57), which will be present for nonzero $a$ and/or nonzero $c$. The shape of that surface, on the other hand, will clearly depend on those parameters, as Fig. 6 shows, and so will the growth shapes. We show in Fig. 9 the physical solution for $a = 0$ and $c = 1$, where points on the circle $(v_1 - 1)^2 + v_2^2 = \frac{1}{4}$ have the maximum growth rate. The full asymmetric case of the model (50) is shown in Fig. 10 for $a = 0.25$ and $c = 1$. In this case it turns out that the saddle point of $\mathrm{Re}[f]$ contributes at $v_1 = 1.125$ whereas the maximum growth rate is at $v_1 = 0.5$.

It is interesting to observe that in the radially symmetric case the saddlelike branch of $\lambda^r(\vec{v})$ is not present. The way in which it disappears when $a \to 0$ and $c \to 0$ in our model is through the divergence of the curvatures of the saddle in both directions. Loosely speaking, the solution goes to $-\infty$ in the $v_1$ axis and $+\infty$ in the $v_2$ axis.

We finally show in Fig. 11 some results of numerical integration of our model. We find good agreement between the calculated and the numerical values of quantities like

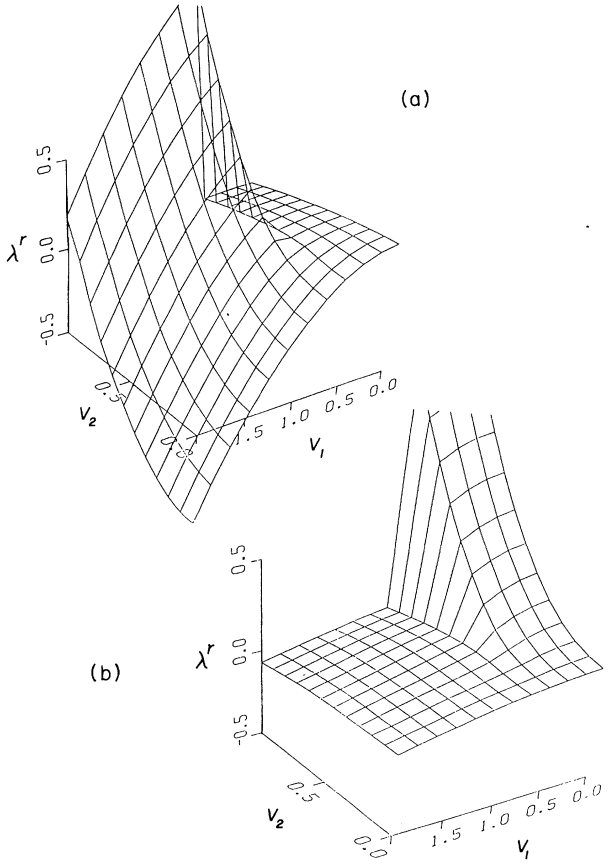


FIG. 7. $\lambda^r(\vec{v})$ for $a = 0.25$ and $c = 0$ obtained from (a) the parabolic solution and (b) the second solution in Fig. 6(a).

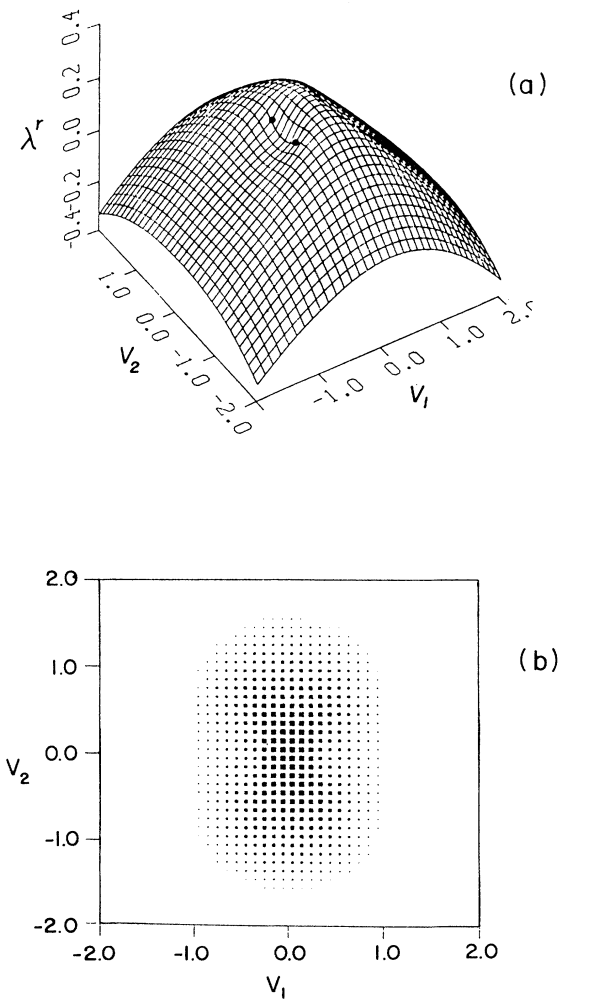


FIG. 8. (a) Physical solution $\lambda^r(\vec{v})$ for $a = 0.25$ and $c = 0$. The branch points are marked by dots. (b) Density plot corresponding to the figure in (a). Only positive values are shown.

the maximum growth rate of the packet and the wavelength of the oscillations present in the patterns. In the discussions in the previous paragraphs, only the real part of $\lambda(\vec{v})$ was considered. The imaginary part adds oscillations to the profile as can be seen in the figures.

## II. NONLINEAR EFFECTS

So far we have discussed a class of unstable *linear* partial differential equations in two spatial dimensions and the various types of asymptotic growth shapes which an initially localized disturbance governed by these equations can have. The next step in this phenomenological approach is the inclusion in our model of nonlinear effects. We shall only consider nonlinear terms which tend to stabilize the equations and restrain the exponential divergence of the linear part. If only small amplitude disturbances are present at the laminar-turbulent interface, nonlinear effects are not expected to change the asymptotic growth shape of the linear theory significantly. We shall give examples where this is the case, and also show how it can break down by the occurrence of shocklike disturbances at the interface.

The inclusion of nonlinear effects in linear models can be done in various ways with various purposes. Since we are interested in the generation of *turbulent spots* we shall select such nonlinearities which, although quenching the exponential divergence of the field, will still allow turbulent fluctuations inside the spot. We shall discuss two different approaches: first, the addition to the linear equations of nonlinear terms in the field $u$ and, second, the use of a nonlinear mapping with discrete versions of the previous models. When speaking of "turbulent spots" we must explain precisely what we mean. By "turbulent" we mean that there is at least one positive Lyapunov exponent. Since the fields in question will be strongly spatially disordered this will in fact imply a whole spectrum of positive Lyapunov exponents with a number growing in proportion to the size of the spot. Now, Lyapunov exponents are usually defined as "ergodic" quantities: on a chaotic attractor any initial condition will return arbitrarily close to itself and thus we can ensure, by sufficiently many iterations, that the spreading rate is averaged over the whole attractor and does not depend on the initial condition. In the present case this is not possible. The spot is strictly speaking not

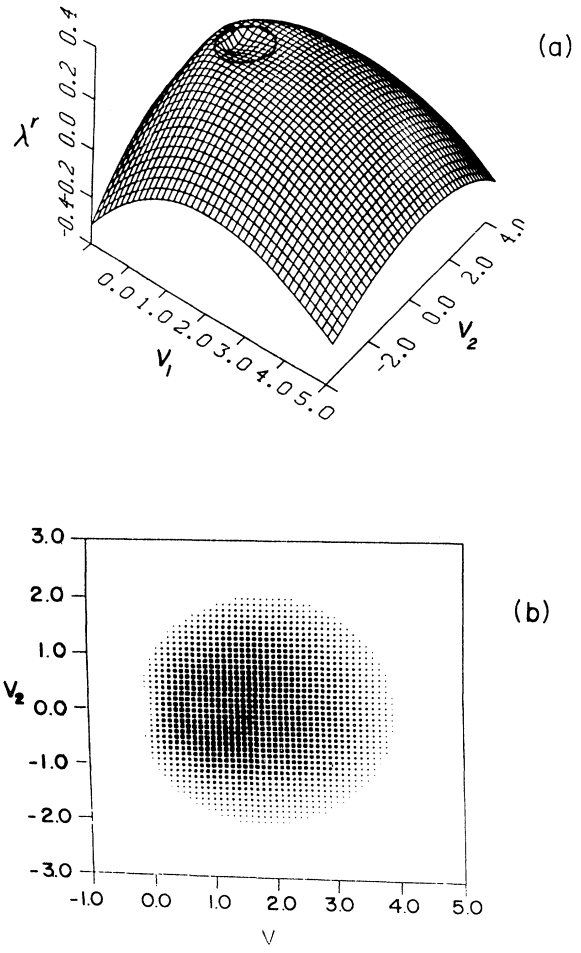


FIG. 9. Same as Fig. 8 for $a = 0$ and $c = 1$. The circle of maximum growth is drawn in (a).

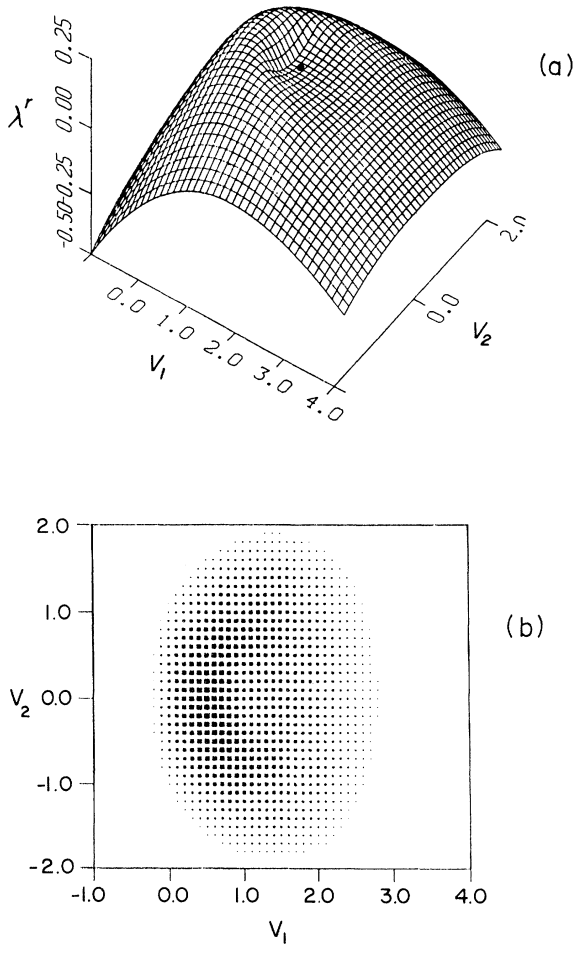


FIG. 10. Same as Fig. 8 for $a = 0.25$ and $c = 1$. The saddle point is marked in (a).

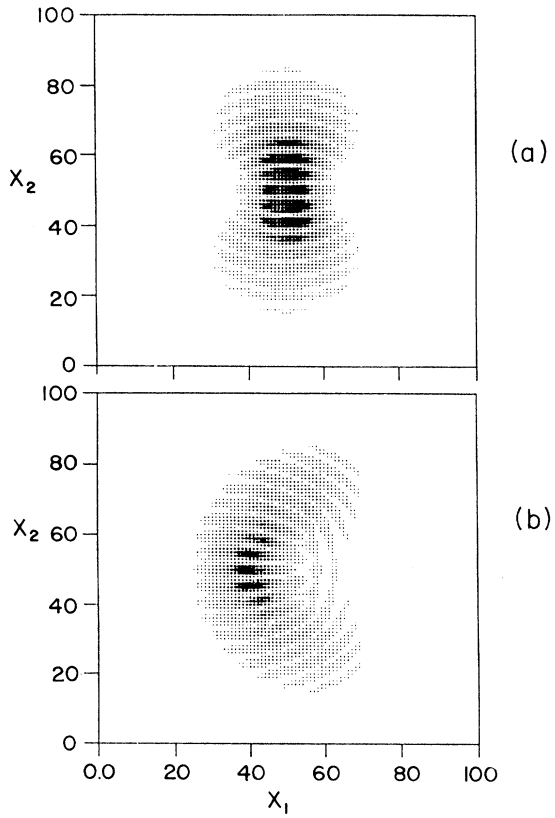


FIG. 11. Density plots from the numerical integration of the model with $\phi$ in (50) for (a) $a = 0.25$ and $c = 0$ and (b) $a = 0.25$ and $c = 1$.

an attractor since it is always expanding. For sufficiently large spots we believe, however, that the chaotic behavior inside the spot is largely independent of its size. Thus we want to compute an average spreading rate of initial conditions *inside* the spot. One has to bear in mind that the medium outside the spot is unstable and will make initial conditions spread exponentially in a trivial way. To avoid this we have to ensure that the Lyapunov vector has support only inside the spot at all times. As we shall see in the following this leads to positive Lyapunov exponents and since they are quite independent of time and typically an order of magnitude smaller than the instability exponent outside the spot [the maximal value of $\lambda(v)$] we believe that our procedure makes sense, although it would clearly be useful to have a rigorous theory for such expanding chaotic systems.

One model known to give chaotic behavior is the (generalized) Kuramoto-Sivashinsky equation (59), variants of which occur widely in nonlinear systems such as surface waves, chemical reactions, or flame fronts. Thus we take as our model

$$\frac{\partial u}{\partial t} = L_0\{u\} + L_1\{u\} + d_1\left(\frac{\partial u}{\partial x_1}\right)^2 + d_2\left(\frac{\partial u}{\partial x_2}\right)^2, \tag{58}$$

where $L_0\{u\}$ and $L_1\{u\}$ are the linear terms given in (2) and (3), and $d_1$ and $d_2$ are constants. Note that by differentiation with respect to the spatial variables (e.g., $x_1$) one gets Burgers-like equations with nonlinearities of the form $u\frac{\partial u}{\partial x_i}$. We shall consider two different cases: $\chi = 0$ and $\chi \neq 0$, which give rise to completely different behaviors.

### A. The case $\chi = 0$

We shall first consider the case in which the constant $\chi$ in (2) is zero. In this case the model has an "interface symmetry:" invariance with respect to $u \to u + \text{const}$. This means that the field will tend to grow in the direction specified by the sign of the nonlinear term. We have recently studied the analog model in one dimension [7], and before going on to the two-dimensional case (58) we shall give a short description of the pertinent results of that work.

#### *1. The one-dimensional case*

Let us consider the one-dimensional partial differential equation (PDE)

$$\frac{\partial h}{\partial t} = -\nabla^2 h - \nabla^4 h + c\nabla^3 h + (\nabla h)^2. \tag{59}$$

For the linear part, calculations analogous to the ones of Sec. I C give the convective exponent $\lambda(v)$. The boundaries of the spot are given by the zeros of $\lambda(v)$ and for $c = 0$ these are $v_f \approx \pm 1.6$. For nonzero $c$ the forward and the backward fronts move with different velocities. Thus $v_f^- \approx -1.4$ and $v_f^+ \approx -1.8$ for $c = 0.1$.

In Fig. 12 we show the result of integrating (59) numerically with initial conditions given by a narrow Gaussian and with $c = 0$. The system size was $L = 10\,000$ and the integration was performed up to a total time $T = 3000$. Figure 12(a) shows three snapshots at equally spaced intervals of time and, as can be seen explicitly from Fig. 12(b), the initial bump clearly approaches a constant *growth shape* [19], i.e., asymptotically the overall shape of $h(x,t)$ is given by

$$h_{sh}(x,t) = tH(x/t), \tag{60}$$

where $H$ is *independent* of time. The bump grows sideways with velocity $v_f \approx 1.60$ in accordance with the linear result above and upward with a velocity $v_0 \approx 0.43$ in agreement with the numerically estimated mean velocity for a large, homogenous system. Note that this type of "growth shape" is different from the one used earlier in this paper. Here it is a shape in the field direction, whereas earlier it was a shape in $(x_1, x_2)$ space. To distinguish them, we shall refer to the present growth shapes as "nonlinear."

From Fig. 12(b) we see that the growth shape is well approximated by a central parabolic part joined with continuous $\nabla h$ — but discontinuous $\nabla^2 h$ — to straight edges nearer to the fronts. We observe that, if a small amount of noise is added to the initial Gaussian, the macroscopic shape is unaltered although the exact microscopic mirror symmetry is lost. Indeed, all localized initial conditions that we have tried seem to evolve into the same macroscopic growth shape.

When the overall shape (60) is subtracted from $h(x,t)$ the field shows strong fluctuations (Fig. 13) whose statistical properties seem indistinguishable from the solutions of (59) grown from uniformly random initial conditions, except for short regions around the fronts. As in the homogeneous system, the $h$ field is clearly chaotic. When computing Lyapunov exponents [20], as mentioned above, one has to keep in mind the strong linear divergence of the flat state. To avoid this, Lyapunov vectors with support inside the growth region must be used exclusively, and this is accomplished most easily by taking initial conditions for the Lyapunov vector with support only in the initial seed. In this way the Lyapunov vector spreads with the spot and we found the largest Lyapunov exponent for the growing shape to be identical to that of a large homogenous system.

When the value of $c$ is nonzero, the $x \to -x$ symmetry is broken and the initial bump approaches an asymmetric growth shape, as shown in Fig. 14(a) for $c = 0.1$. It can nevertheless be well approximated by the same central parabolic part and the two straight edges as in the case $c = 0$. For larger values of $c$, however, the system shows a new type of instability. Figure 14(b) shows the result

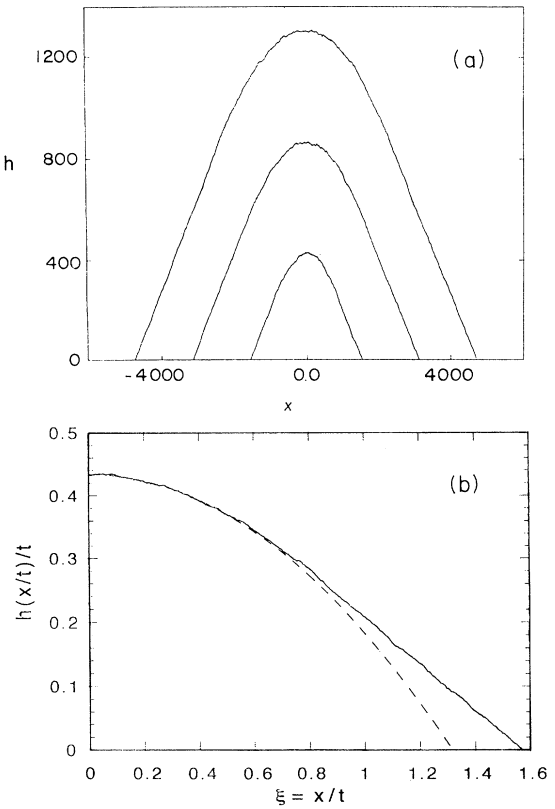


FIG. 12. Numerical solution of the Kuramoto-Sivashinsky equation with an initial seed. The grid spacing was 0.5. (a) The solution is shown at times $t_1 = 1000$, $t_2 = 2000$, and $t_3 = 3000$. (b) The solutions at the three times of (a) are superimposed by the scaling $h \to h/t$ and $x \to x/t$. Due to the mirror symmetry only positive $x$ are shown. The dashed curve is the parabola $y(\xi) = 0.434 - 0.25\xi^2$.

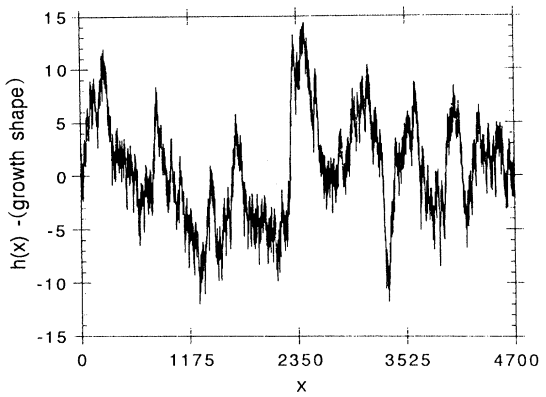


FIG. 13. Remaining field after the growth shape is subtracted from $h(x,t)$, for a fixed time ($t = 3000$) as a function of $x$.

of the numerical integration of (59) for $c = 0.2$. The right-hand part of the growth shape is still well defined, but the left-hand part now consists of a series of steps, in which, clearly, our numerical solution is insufficient.

To find the nonlinear growth shape and understand this instability we shall make the following ansatz

$$h(x,t) = tH(x/t) + g(x,t), \tag{61}$$

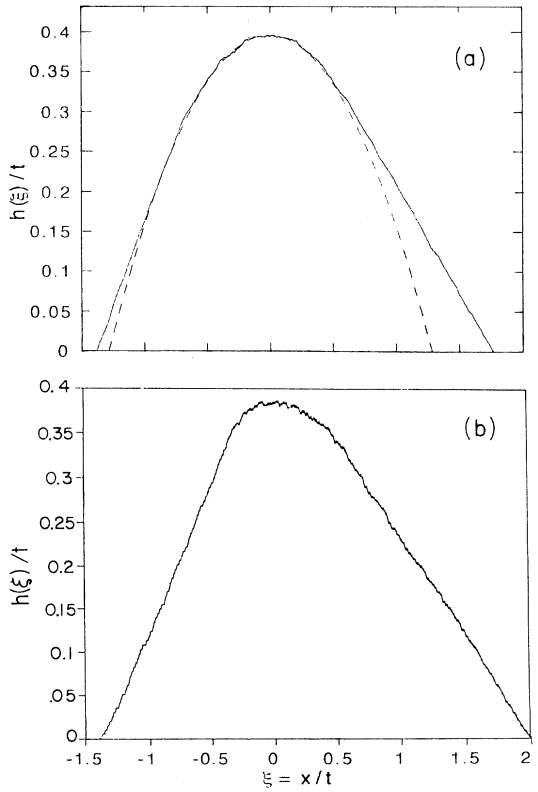


FIG. 14. Numerical solution of (59). The field and the spatial variable have been scaled as $h \to h/t$ and $x \to x/t$. (a) $c = 0.1$. The dashed curve is the parabola $y(\xi) = 0.396 - 0.24\xi^2$. (b) $c = 0.2$. Note the step structure on the left side.

where we shall also assume that $g$ has no growth rate of its own, i.e., $\langle \dot{g} \rangle = 0$. Inserting (61) into (59) and taking the limit $t \to \infty$ — since we are interested in the asymptotic growth shape — gives

$$\frac{\partial g}{\partial t} = A(\xi) - \nabla^2 g - \nabla^4 g + c\nabla^3 g + (\nabla g)^2 + 2H'(\xi)\nabla g, \tag{62}$$

where $\xi = x/t$ and $A(\xi) = [H'(\xi)]^2 + \xi H'(\xi) - H(\xi)$ and where the neglected terms are $O(1/t)$. For very large $t$ we can think of $\xi$ as a slowly varying variable, essentially constant over a wide range of $x$ (in fact, $\frac{d\xi}{dx} = \frac{1}{t}$). In that case, (62) differs from (59) only by a constant $A(\xi)$ and a linear term in $\nabla g$: $2H'(\xi)\nabla g$. But such linear terms can be removed by a Galilean transformation, i.e., by going into a moving frame, which should not alter the growth rate of $g$. Now, Eq. (59) with homogeneous boundary conditions in a sufficiently large system has growth rate $v_0(c)$. Thus, in order for $g$ to have zero growth rate, we must have

$$A(\xi) = [H'(\xi)]^2 + \xi H'(\xi) - H(\xi) = -v_0(c). \tag{63}$$

This equation is our old friend, the Clairaut equation [like (7)], whose general solution is given by the one-parameter family of straight lines $H_a(\xi) = a\xi + a^2 + v_0(c)$. There is also a singular solution with no arbitrary constants which is given as the envelope of the family of straight lines. Now, the boundary conditions on (63) are $H(0) = v_0(c)$ and — from the linear theory — that $H(\xi) \to 0$ at the edges $\xi = v_f^{\pm}$. These, together with the demand that $H$ be smooth determine $H$ as

$$H(\xi) = v_0(c) - \frac{1}{4}\xi^2 \tag{64}$$

for small $\xi$. This parabolic shape, which is the singular solution of (63), is valid in the interval $\xi_- < \xi < \xi_+$, where $\xi_- = v_f^- + \sqrt{(v_f{}^-)^2 - 4v_0(c)}$ and $\xi_+ = v_f^+ - \sqrt{(v_f{}^+)^2 - 4v_0(c)}$. At $\xi = \xi_\pm$ the shape has a discontinuity in the curvature and becomes linear — one of the straight lines in the family above — all the way out to $\xi = v_f^\pm$ as shown in Fig. 15(a). In other words, the shape is found by joining the inner parabola to its tangents [the ones that go through $(v_f^\pm, 0)$, as determined by linear theory]. We observe that the velocity of the moving frame $|v| = 2|H'(\xi)| \le |\xi_\pm|$ is never outside of the growth region $[v_f^-, v_f^+]$, where $A(\xi)$ would be zero and not $-v_0(c)$. Thus the solution is self-consistent.

The construction described above cannot necessarily be done, however. When $c$ is nonzero, say positive, the velocities $v_f^\pm$ will both have a positive increment indicating that the disturbance is moving towards positive $x$ while it spreads in the laminar environment. This means that the allowed growth region $[v_f^-, v_f^+]$ will be displaced with respect to the center of the parabola in (64) and if $c$ is large enough none of the tangents on the left side will lie within that region. Presumably the growth shape should then be parabolic all the way down to $\xi = v_f^-$, where it should, discontinuously, jump to 0 as shown in Fig. 15(b). The meaning of such a growth shape is not clear and presumably gives rise to an instability in the system, although it is not easy to simulate numerically. Within our numerical accuracy, a steplike structure appears on the left-hand side [Fig. 14(b)], which makes the linear stability results irrelevant. The left propagating edge is clearly "nonlinear" and moves with a velocity $v_f^- \approx -1.4$, overshooting the velocity $-1.23$ predicted by the linear theory. The smallest value of $c$ at which this happens can be found from $v_f^-(c) = -2\sqrt{v_0(c)}$, which corresponds to $\xi_- = v_f^-$, but with the parabolic behavior all the way down to the edge. The velocity $v_f^-(c)$ can be computed explicitly as mentioned above, but $v_0(c)$ is only known numerically. We thus find the critical value $c_r$ to be slightly above 0.1 in agreement with our direct numerical findings.

One can find the nonlinear growth shapes in terms of average growth velocities [19], which, as we shall see, is totally equivalent to the previous formulation. Here one assumes that effectively

$$\frac{\partial h}{\partial t} = v(\nabla h), \tag{65}$$

where $v(\nabla h)$ is the slope-dependent growth velocity. Again Galilean invariance can be used to relate growth rates for systems with different mean slopes. The invariance of (59) under the simultaneous Galilean transforma-

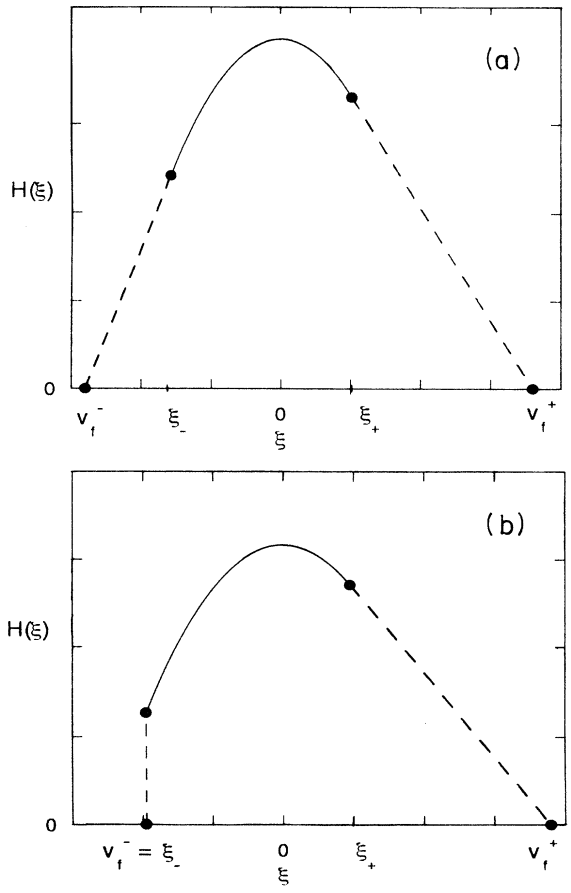


FIG. 15. Schematic drawing of growth shapes (a) for $c < c_r$ and (b) for $c > c_r$.

tion $x' = x - 2ut$, $t' = t$, and a tilt $h = h' - ux' - u^2t'$, all with $u$ =const, implies that the average growth rate $v = \langle \frac{\partial h}{\partial t} \rangle$ at a fixed macroscopic inclination $u = \langle \frac{\partial h}{\partial x} \rangle$ is given by $v(u) = v_0(c) + u^2$. We then look for a stationary growth shape, which is a solution to (65) with the scaling form given in (60). Using $v(u) = v_0(c) + u^2$, we obtain the equation for $H(\xi)$ given in (63).

### 2. *The two-dimensional case*

We now return to the two-dimensional case given by (58). In analogy with the methods of the last section we shall formulate the problem in terms of a slope-dependent growth velocity $v$. We assume that, effectively,

$$\frac{\partial u}{\partial t} = v\left(\frac{\partial u}{\partial x_1}, \frac{\partial u}{\partial x_2}\right). \tag{66}$$

The invariance of (58) under the simultaneous transformation $u = u' + \vec{w} \cdot \vec{x}$, $x_i = x'_i - 2d_i w_i t$ (with $w_i$ =const) implies that the average growth rate at a fixed macroscopic inclination is given by $v(w_1, w_2) = v_0 + d_1 w_1^2 + d_2 w_2^2$, where $v_0$ is the growth velocity at zero slope, which depends on all the parameters in Eq. (58). If we now look for a stationary growth shape, which is a solution to (66) with the scaling form

$$u(\vec{x}, t) = tU\left(\frac{\vec{x}}{t}\right), \tag{67}$$

we obtain the Clairaut equation

$$U(\vec{\xi}) = \vec{\xi} \cdot \vec{\nabla}_{\vec{\xi}} U + v\left(\frac{\partial U}{\partial \xi_1}, \frac{\partial U}{\partial \xi_2}\right), \tag{68}$$

where the expression for $v$ is given above. The general solution is given as a two-parameter family of planes and the singular solution is their envelope [14]

$$U_s(\xi_1, \xi_2) = v_0 - \frac{{\xi_1}^2}{4d_1} - \frac{{\xi_2}^2}{4d_2}. \tag{69}$$

The next step is to adjust the solutions to the boundary conditions that $U(\xi_1, \xi_2)$ should go to zero at points $(\xi_1, \xi_2)$ defining the growth shape (as determined from the linear theory). We then find that $U$ is given by (69) in a region of the $(\xi^1, \xi^2)$ plane around $\vec{\xi} = \vec{0}$ joined to its tangent planes — the ones whose intersection with the $(\xi^1, \xi^2)$ plane is a tangent to the growth shape. This solution is the two-dimensional version of the solution shown in Fig. 15(a), which can be thought of as a view of the surface cut through the origin.

As in the one-dimensional case, however, the nonlinear growth shapes cannot necessarily be adjusted to the linear ones. For definiteness, we shall take in the remainder of this section, as the linear part of our model in (58), the model discussed in the previous section and defined in (50). The different growth shapes generated by that linear model can be seen in Figs. 8–10. With the choice $\chi = 0$, we cannot capture the structure in the upper part of the surfaces $\lambda^r(\vec{v})$ and the growth shapes will be simple curves. In particular, for the case $a \neq 0$ to which we shall confine our attention, the shape will be elongated in one direction.

We first discuss the case $c = 0$, for which the elongated shape will be centered at the origin. Varying the constants $d_1$ and $d_2$ in (58), it is *always* possible to adjust the linear and nonlinear growth shapes (69): if $a$ is positive, for example, the shape will be elongated in the $v_2$ direction and we choose $d_1 < d_2$. We show in Fig. 16 the results of numerical integration of (58) with $a = 0.25$, $d_1 = 0.25$, and $d_2 = 0.5$. As can be seen, there is a well-defined growth shape $U(\vec{\xi})$, which can be explained by the construction described above. One should note that $d_1$ and $d_2$ have the same sign (here chosen positive). If they are both negative the transformation $u \to -u$ will take us back to the former case. The equation with opposite signs in $d_1$ and $d_2$ seems always to diverge.

When $c$ is nonzero, the elongated shape defining the allowed growth region will be displaced with respect to the origin, and if $c$ is large enough none of the planes which are tangent to (69) will lie within that region. We again have an instability in the system, which will

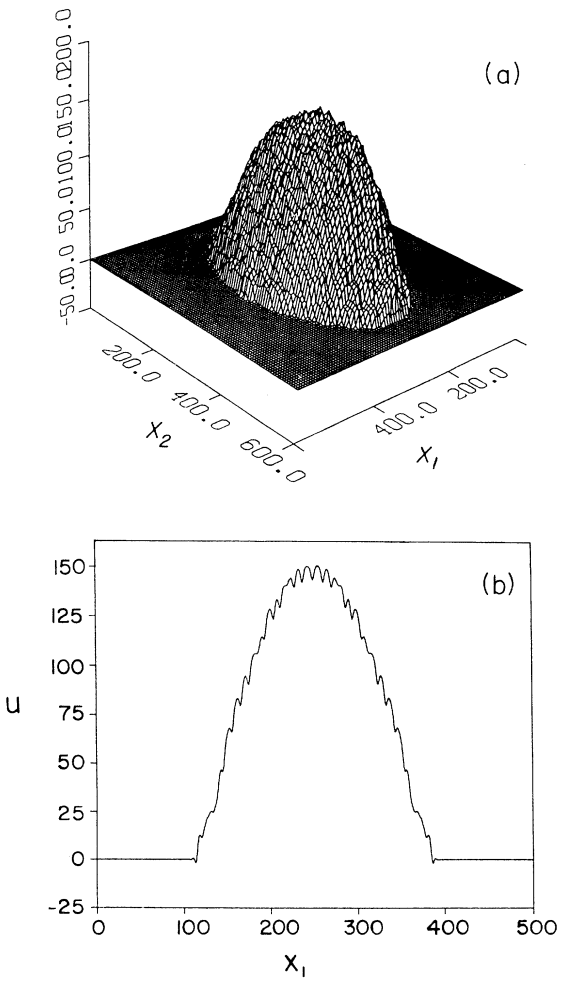


FIG. 16. (a) $u(x_1, x_2)$ obtained from the numerical integration of (58) for $a = 0.25$, $c = 0$, $d_1 = 0.25$, and $d_2 = 0.5$. (b) The cut $u(x_1, x_2 = 0)$.

give rise to the same kind of steplike structure found earlier, making the linear stability results irrelevant. We show in Fig. 17 the results for $a = 0.25$, $c = 0.5$, $d_1 = 0.25$, and $d_2 = 0.75$, which is the two-dimensional analog of Fig. 14(b). The smallest value of $c$, say positive, at which the instability happens can be found from $v_1^-(c) = -2\sqrt{d_1 v_0(c)}$, where $(v_1^-(c), v_2 = 0)$ is a point on the growth shape $[v_1^-(c) < 0]$ and $v_0(c)$ can be found numerically.

### B. The case $\chi \neq 0$

When we consider $\chi$ in (2) different from zero, we break the invariance of $u$ with respect to the transformation $u \to u' +$ const. Now $\frac{\partial u}{\partial t}$ depends on the value of $u$ itself and not only on its derivatives as before. This means that if $|u|$ becomes large the term $\chi u$ will dominate and, depending on its sign, $u$ will increase or decrease exponentially. Therefore we *cannot* obtain a scaling form as given in (67) according to which the asymptotic growth of $u$ is linear in time. We shall see, however, that for nonzero $\chi$ we can still generate turbulent spots, where the divergent field inside the spot is replaced by *chaotic* or *turbulent* motion.

We shall confine our attention to negative values of $\chi$ in (58) since for any positive $\chi$ the model diverges. Such a model with $c = 0$ was studied earlier in one spatial dimension in the context of spatiotemporal intermittency [21]. We further assume that $\chi > -\frac{1}{4}$ so that the linear part of the model given in (50) is unstable. With such a choice, the growth shapes from linear theory can reveal more of the complex structure present in the upper part of $\lambda^r(\vec{v})$ shown in Figs. 8(a)–10(a).

In order to generate "turbulent spots," we will look at the full asymmetric case of the model (50), i.e., $a \neq 0$ and $c \neq 0$, which *can* generate concave growth shapes. In particular, this is true for the values $a = 0.25$ and $c = 1$. From the transition sequence shown in Fig. 5, we can see that the concave shape is obtained from level curves which are higher than the value of $\lambda^r$ at the saddle point $\lambda_S^r$ — or equivalently for $\chi < -\lambda_S^r$. Moreover, as can be seen from the convective exponent $\lambda^r(v_1, v_2 = 0)$ in Fig. 6(c), the disturbance can be convectively unstable for such high level curves, and in this case the rear and the front velocities of the disturbance can be found from (57) as

$$v_1^{\pm} = \frac{1 \pm \sqrt{2(1 - 4\chi)}}{2}. \tag{70}$$

In Fig. 18 we show the results of numerical integration of (58). In the linear part (50) we have $a = 0.25$, $c = 1$, and $\chi = -0.15$, which gives $v_1^- \approx 0.05$ and $v_1^+ \approx 0.95$. The nonlinear term has $d_1 = d_2 = 1$. The spot is convectively unstable and moves through the laminar medium ($v = 0$) with a velocity $v \approx 0.5$. Moreover, the field $u$ inside the spot is chaotic with a small positive Lyapunov exponent ($\approx 0.05$). As noted earlier, when computing the Lyapunov exponent for the disturbance one has to keep in mind that the $u = 0$ state is linearly unstable with an instability exponent $\chi + \frac{1}{4}$ and thus use

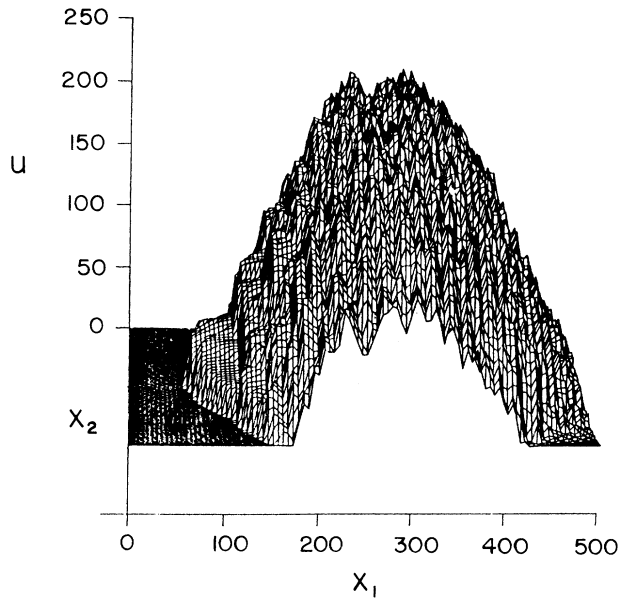


FIG. 17. $u(x_1, x_2)$ obtained from the numerical integration of (58) for $a = 0.25$, $c = 0.5$, $d_1 = 0.25$, and $d_2 = 0.75$.

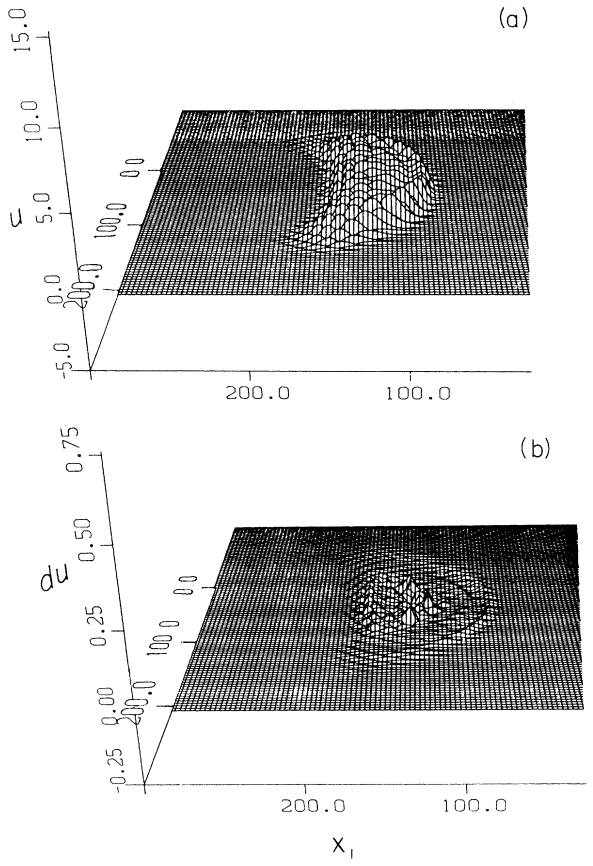


FIG. 18. (a) $u(x_1, x_2)$ obtained from the numerical integration of (58) for $a = 0.25$, $c = 1$, $\chi = -0.15$, $d_1 = 1$, and $d_2 = 1$. (b) Lyapunov vector for the same conditions.

Lyapunov vectors with support inside the growth region only. As in the one-dimensional (1D) case, this can be accomplished by taking initial conditions for the Lyapunov vector with support only in the initial localized disturbance. Indeed, the Lyapunov vector corresponding to the spot in Fig. 18(a), for such initial conditions, remains confined to the region where the spot is, as can be seen from Fig. 18(b).

### C. The nonlinear mapping

A different approach to localized turbulent spots was presented some years ago in [22]. Here a discrete set of coupled nonlinear maps was introduced, which created a chaotic repeller in the system. Thus we take a lattice of coupled maps of the form

$$u(\vec{x}_i, n+1) = u(\vec{x}_i, n) + L_0^{(d)}\{u\} + L_1^{(d)}\{u\} + f(u). \tag{71}$$

Here, $\vec{x}_i$ and $n$ are the discrete spatial coordinate and discrete time, respectively, and $L_0^{(d)}$ and $L_1^{(d)}$ are discrete versions of the operators in (2) and (3). The last term is a nonlinear function $f$, designed to have a chaotic repeller away from $u = 0$. For small $u$, $f$ is the identity such that the linear stability properties are given by $L_0^{(d)}$ and $L_1^{(d)}$.

We shall consider the case where the linear system is absolutely stable, although *convectively* unstable. In analogy with [22] we shall choose a nonlinear map $f : [-1,1] \to [-1,1]$, which is piecewise linear

$$f(x) = \begin{cases} 3x+2 & \text{if} \quad -1 \le x < -1/3 \\ x & \text{if} \quad -1/3 \le x \le 1/3 \\ 3x-2 & \text{if} \quad 1/3 < x \le 1. \end{cases} \tag{72}$$

For such a one-dimensional mapping the dynamics are interesting only outside the interval $[-1/3, 1/3] = J$, where $f$ has a chaotic repeller $\Lambda = \{x \in [-1,1] : f^n(x) \notin J \forall n \ge 0\}$. Due to the presence of such a repeller, orbits of $f$ outside $J$ are unstable and will undergo a chaotic excursion before they can escape from $\Lambda$ back into that interval. Once $x$ is reinjected into $J$, the dynamics will be governed by the linear part $f(x) = x$.

When the overall dynamics are considered, an initially localized small disturbance $u_0$ will grow and spread itself as described in the previous sections since the low amplitude instability is completely determined by (71). When $u(\vec{x}_i, t)$ becomes sufficiently large so that it falls outside the interval $J$, it will undergo a chaotic excursion due to the presence of the chaotic repeller. However, due to the strong coupling introduced by the equation involving also next nearest neighbors, the chaotic trip is much shorter than it would be for the mapping alone or even for the model considered in [22] and $u(\vec{x}_i, t)$ is reinjected back into $J$. Once there, the dynamics at this site will again be controlled by (71) and the value of $u$ will grow until either it escapes again or one of its near neighbors escapes from $J$, causing a small decrease in the value of $u$. This behavior is seen in Fig. 19, where we show $u$ as a function of time at a fixed site $\vec{x}_i$. Here the linear part is (50) with $a = 0.25$, $c = 1$, and $\chi = -0.15$.

The outcome of the dynamics described above is the development of a disturbance with the same growth shape as the one obtained in the linear model, but bounded in amplitude, as shown in Fig. 20. The growth shape is kept invariant since only small amplitude disturbances are present at the boundary, which are not directly affected by the mapping. Moreover, the oscillations in the profile are still present. They are strong correlations which originate from the linear equation and are insensitive to the mapping. On the smaller scales, on the other hand, the linear equation is ineffective — it is unstable only for a range of wave numbers around the origin — and the structure is erratic due to the mapping.

We observe that, even though $f$ maps the interval $[-1,1]$ onto itself, the equation is unstable and it is possible that some of the iterates will escape from that interval, although very rarely. For those iterates, it is enough, in order to bring them back to $J$, to extend the interval over which the mapping acts just by stretching the external limits $-1$ and 1 in (72). Again, the strong coupling will dominate the dynamics, keeping the values of the amplitude mostly restricted to the interval $J$.

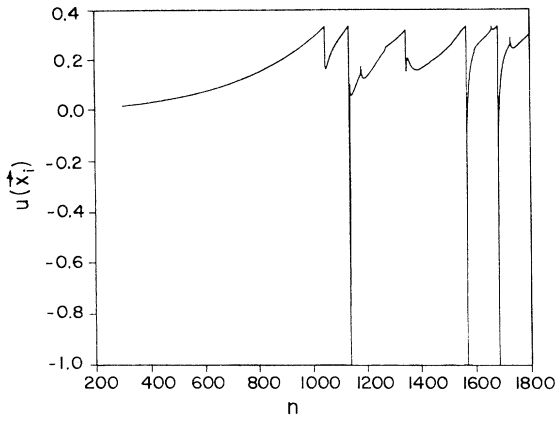


FIG. 19. Time evolution of $u$ in a point $\vec{x}_i$ of the lattice for $a = 0.25$, $c = 1$, and $\chi = -0.15$.

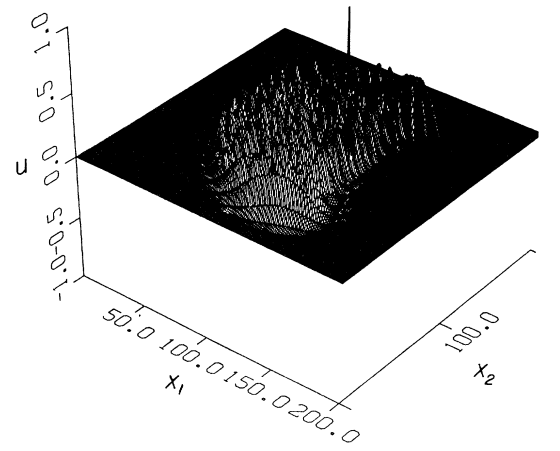


FIG. 20. Turbulent spot from the map (71) for $a = 0.25$, $c = 1$, and $\chi = -0.15$.

## ACKNOWLEDGMENTS

We would like to thank David Rand and Jakob Bondorf for helpful comments. C.V.C. acknowledges support from CNPq–Conselho Nacional de Desenvolvimento Científico e Tecnológico (Brazil) and T.B. thanks Novo Nordisk Fonden for support.


## APPENDIX: THE CRITICAL POINTS OF $\lambda(\vec{v})$

In order to estimate the integral in (51) for large $t$, we find all the saddle points of the function $f(\vec{q})$ in the exponent and evaluate the integrand at the saddle point which gives the largest contribution, provided that the contour can be deformed through that saddle. Now suppose that the saddle point contributing at a given velocity is real. Then, this point must be a critical point of the real part of $f$ as a function of real $\vec{q}$. Moreover, the corresponding value of $\vec{v}$ will be a critical point of $\lambda^r(\vec{v})$ since $\vec{\nabla}_{\vec{v}}\lambda(\vec{v}) = -i\vec{q}$. We now show that the behaviors of $\lambda^r(\vec{v})$ around the critical point $\vec{v}_0$ and $\mathrm{Re}[f(\vec{q})]$ around the corresponding critical point $\vec{q}_0(\vec{v}_0)$ are the same.

We start by writing $f(\vec{q})$, where $\vec{q}$ is a real vector, as $R(\vec{q}) + i[\vec{q}\cdot\vec{v} + I(\vec{q})]$. The behavior of $R(\vec{q})$ around its critical point $\vec{q}_0$ can be determined from the evaluation of the expression

$$\Delta_R = R_{11}R_{22} - (R_{12})^2 \tag{A1}$$

at the critical point. Here, $R_{ij}$ simply means $\frac{\partial^2 R}{\partial q_i \partial q_j}$, a notation which we shall adopt also for first derivatives and for $I$ and $\lambda^r$ as well. Now, if $\Delta_R$ is positive, $\vec{q}_0$ will be a maximum if $R_{ii} < 0$ or a minimum if $R_{ii} > 0$. For negative $\Delta_R$, $\vec{q}_0$ will be a saddle point. Finally, if $\Delta_R = 0$, the methods for the determination of the nature of the critical point become more complex.

In order to find the behavior of $\lambda^r(\vec{v})$ around $\vec{v}_0$, we now calculate $\Delta_\lambda$, which is defined in the same way as $\Delta_R$ in (A1). So we need the quantities $\lambda^r_{ij}$ which are given by

$$\frac{\partial^2\lambda^r}{\partial v_i \partial v_j} = -\frac{\partial q_i^i}{\partial v_j} = -\frac{\partial q_j^i}{\partial v_i}, \tag{A2}$$

where $q_j^i$ is the component $j$ of the imaginary part of $\vec{q}$. Now, the dependence of $\vec{q}$ on $\vec{v}$ is determined from

$$\begin{aligned} &R_1 + i(v_1 + I_1) = 0, \\ &R_2 + i(v_2 + I_2) = 0, \end{aligned} \tag{A3}$$

which are the equations for the saddle points. For a change $d\vec{v}$ in $\vec{v}_0$, there will be a corresponding change $d\vec{q} = d\vec{q}^r + id\vec{q}^i$ in $\vec{q}_0$, which can be found from (A3) as the following linear system:

$$\begin{aligned} &R_{11}dq_1^r + R_{12}dq_2^r - I_{11}dq_1^i - I_{12}dq_2^i = 0, \\ &R_{12}dq_1^r + R_{22}dq_2^r - I_{12}dq_1^i - I_{22}dq_2^i = 0, \\ &I_{11}dq_1^r + I_{12}dq_2^r + R_{11}dq_1^i + R_{12}dq_2^i = -dv_1, \\ &I_{12}dq_1^r + I_{22}dq_2^r + R_{12}dq_1^i + R_{22}dq_2^i = -dv_2, \end{aligned} \tag{A4}$$

where $R_{ij}$ and $I_{ij}$ are evaluated on the real saddle point $\vec{q}_0$. We will be interested in solving (A4) for $dq_1^i$ and $dq_2^i$ since they are the quantities appearing in (A2). When this is done, we obtain

$$\begin{aligned} \frac{\partial q_1^i}{\partial v_1} &= -\frac{1}{D_0}\left(R_{22} + \frac{I_{12}C}{\Delta_R} + \frac{I_{22}D}{\Delta_R}\right), \\ \frac{\partial q_1^i}{\partial v_2} &= \frac{1}{D_0}\left(R_{12} + \frac{I_{11}C}{\Delta_R} + \frac{I_{12}D}{\Delta_R}\right), \\ \frac{\partial q_2^i}{\partial v_1} &= \frac{1}{D_0}\left(R_{12} + \frac{I_{12}A}{\Delta_R} + \frac{I_{22}B}{\Delta_R}\right), \\ \frac{\partial q_2^i}{\partial v_2} &= -\frac{1}{D_0}\left(R_{11} + \frac{I_{11}A}{\Delta_R} + \frac{I_{12}B}{\Delta_R}\right), \end{aligned} \tag{A5}$$

where

$$\begin{aligned} A &= R_{22}I_{11} - R_{12}I_{12}, \\ B &= R_{11}I_{12} - R_{12}I_{11}, \\ C &= R_{22}I_{12} - R_{12}I_{22}, \\ D &= R_{11}I_{22} - R_{12}I_{12}, \end{aligned} \tag{A6}$$

and

$$D_0 = \frac{1}{\Delta_R}(\Delta_R^2 + \Delta_I^2 + A^2 + 2BC + D^2), \tag{A7}$$

with $\Delta_R$ given in (A1) and $\Delta_I$ defined in the same way.

We now can evaluate $\lambda^r_{ij}$ in (A2) and then $\Delta_\lambda = \lambda^r_{11}\lambda^r_{22} - (\lambda^r_{12})^2$, from which we can find the behavior of $\lambda^r(\vec{v})$ around $\vec{v}_0$. It turns out that $\Delta_\lambda$ is simply given by $\frac{1}{D_0}$, where $D_0$ is given in (A7). Now, from (A6) it is easy to show that $AD - BC = \Delta_R\Delta_I$.When this result is used in (A7), we obtain finally that

$$\Delta_\lambda = \frac{\Delta_R}{(\Delta_R - \Delta_I)^2 + (A + D)^2}. \tag{A8}$$

The quantity in the denominator is always positive and therefore $\Delta_\lambda$ and $\Delta_R$ have the same sign. Moreover, it is not difficult to show that for positive $\Delta_R$ (and $\Delta_\lambda$), $R_{ii}\lambda_{jj}$ will also be positive.

Therefore we have shown that the nature of any critical point $\vec{q}_0$ of $\mathrm{Re}[f(\vec{q})]$ — which are also real saddle points of $f(\vec{q})$ — is brought into $\lambda^r(\vec{v})$: not only will the corresponding $\vec{v}_0$ be a critical point, but a critical point of the same kind. Also, it is true that if $\lambda^r(\vec{v})$ has any critical point, the corresponding saddle point must be real and therefore it must be a critical point of $\mathrm{Re}[f(\vec{q})]$. Nevertheless, whether the real saddle point is the one contributing at the corresponding velocity can only be answered through the analysis of all the saddle points in the complex plane.

[1] H. W. Emmons, J. Aeronaut. Sci. **18**, 490 (1951).
[2] J. O. Hinze, *Turbulence* (McGraw-Hill, New York, 1975).
[3] D. J. Tritton, *Physical Fluid Dynamics* (Claredon, Oxford, 1988).
[4] I. Wygnanski, M. Sokolov, and D. Friedman, J. Fluid Mech. **78**, 785 (1976).
[5] B. J. Cantwell, D. Coles, and P. Dimotakis, J. Fluid Mech. **87**, 641 (1978).
[6] A. E. Perry, T. T. Lim, and E. W. Teh, J. Fluid Mech. **104**, 387 (1981).
[7] C. Conrado and T. Bohr, Phys. Rev. Lett. **72**, 3522 (1994).
[8] T. B. Benjamin, J. Fluid Mech. **10**, 401 (1961).
[9] J. Watson, J. Fluid Mech. **14**, 211 (1962).
[10] R. G. Briggs, *Electron Stream Interaction with Plasmas* (MIT, Cambridge, MA, 1964).
[11] L. S. Hall and W. Henckrotte, Phys. Rev. **166**, 120 (1968).
[12] W. O. Criminale, Jr. and L. S. G. Kovasznay, J. Fluid Mech. **14**, 59 (1962).
[13] M. Gaster, J. Fluid Mech. **14**, 222 (1962); **22**, 433 (1965); **32**, 173 (1968).
[14] J. Mathews and R. L. Walker, *Mathematical Methods of Physics* (Benjamin, New York, 1970).
[15] Y. Kuramoto, *Chemical Oscillations. Waves and Turbulence* (Springer, Berlin, 1984).
[16] G. I. Sivashinsky, Acta Astron. **4**, 1177 (1977).
[17] J. Swift and P. C. Hohenberg, Phys. Rev. A **15**, 319 (1977).
[18] G. B. Whitham, *Linear and Nonlinear Waves* (Wiley, New York, 1974).
[19] J. Krug and H. Spohn, in *Solids far from Equilibrium*, edited by C. Godrèche (Cambridge University, Cambridge, England, 1991).
[20] T. Bohr, in *Applications of Statistical and Field Theory Methods to Condensed Matter*, edited by D. Beariswyl, A. R. Bishop, and J. Carmelo (Plenum, New York, 1990), p. 157.
[21] H. Chaté, *Spontaneous Formation of Space-Time Structures and Criticality*, edited by T. Riste and D. Sherrington (Kluwer, Dordrecht, 1991).
[22] T. Bohr and D. Rand, Physica D **52**, 532 (1987).

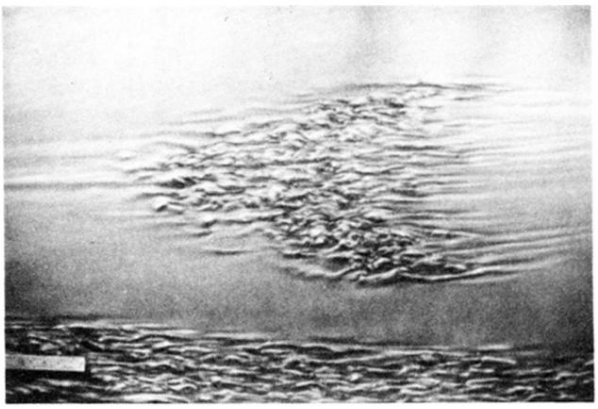

FIG. 1. Turbulent spot in water seen through a wall on which a boundary layer has formed. The flow is from left to right and the visualization by suspended aluminum flakes (from [5]).